The Role of Alkali and Alkaline Earth Metals in the CO$_2$ Methanation Reaction and the Combined Capture and Methanation of CO$_2$

Anastasios I. Tsiotsias [1] [ID], **Nikolaos D. Charisiou** [1], **Ioannis V. Yentekakis** [2] [ID] **and Maria A. Goula** [1,*] [ID]

[1] Laboratory of Alternative Fuels and Environmental Catalysis (LAFEC), Department of Chemical Engineering, University of Western Macedonia, GR-50100 Koila, Greece; antsiotsias@uowm.gr (A.I.T.); ncharisiou@uowm.gr (N.D.C.)

[2] Laboratory of Physical Chemistry & Chemical Processes, School of Environmental Engineering, Technical University of Crete, GR-73100 Chania, Greece; yyentek@isc.tuc.gr

[*] Correspondence: mgoula@uowm.gr; Tel.: +30-24610-68296

Abstract: CO$_2$ methanation has great potential for the better utilization of existing carbon resources via the transformation of spent carbon (CO$_2$) to synthetic natural gas (CH$_4$). Alkali and alkaline earth metals can serve both as promoters for methanation catalysts and as adsorbent phases upon the combined capture and methanation of CO$_2$. Their promotion effect during methanation of carbon dioxide mainly relies on their ability to generate new basic sites on the surface of metal oxide supports that favour CO$_2$ chemisorption and activation. However, suppression of methanation activity can also occur under certain conditions. Regarding the combined CO$_2$ capture and methanation process, the development of novel dual-function materials (DFMs) that incorporate both adsorption and methanation functions has opened a new pathway towards the utilization of carbon dioxide emitted from point sources. The sorption and catalytically active phases on these types of materials are crucial parameters influencing their performance and stability and thus, great efforts have been undertaken for their optimization. In this review, we present some of the most recent works on the development of alkali and alkaline earth metal promoted CO$_2$ methanation catalysts, as well as DFMs for the combined capture and methanation of CO$_2$.

Keywords: CO$_2$ methanation; methanation catalysts; alkali and alkaline earth metal promoters; CO$_2$ capture and utilization; dual-function materials

1. Introduction

Antropogenic CO$_2$ emissions have skyrocketed in the recent century due to the rapidly expanding energy demands of our society [1]. Since increasing concentrations of greehouse gas emissions have the potential to cause irreversible damage to our planet's climate, it is clear that this trend eventually has to be reversed [2,3]. Carbon capture and storage (CCS) technologies aim to mitigate this problem by capturing CO$_2$ from emission sources and then depositing it to underground geological formations [4]. However, CO$_2$ utilization after the initial capture step (Carbon capture and utilization (CCU)) through conversion of CO$_2$ into fuels and useful chemicals, such as methane, syngas, methanol and higher hydrocarbons, should be considered as a more prudent methodology to recycle our carbon sources [5]. Among the conversion products, methane or synthetic natural gas (SNG) is often favoured as it is an energy source with a high caloric content and also because the already existing and extensive natural gas grid can be utilized for its distribution [6]. However, the hydrogen used during the hydrogenation step should be produced using renewable energy sources in order to achieve carbon neutrality. Hope is

offered by the intense research and development in the field of novel photovoltaics and electrolyzers, aiming to drastically lower the costs for the production of renewable hydrogen [7].

CO$_2$ methanation, also known as the Sabatier reaction, is an exothermic reaction that converts CO$_2$ to methane using hydrogen as the reducing agent [8]:

$$CO_2 + 4H_2 \rightleftharpoons CH_4 + 2H_2O, \Delta H_{298K} = -164 \text{ kJ/mol}$$

This reaction has gained increased traction in recent years, since it can be employed to reduce our carbon footprint by recycling existing carbon sources, and it is also considered vital in the facilitation of long term space exploration missions and manned missions to Mars [8,9]. Other possible products besides CH$_4$ during the hydrogenation of CO$_2$ include CO via the reverse water-gas shift (RWGS) reaction [10], methanol (CH$_3$OH) and C$_{2+}$ hydrocarbons with two or more carbon atoms through a promotion of the C–C coupling step [11]. CO$_2$ methanation targets the exclusive production of CH$_4$ over the other possible hydrogenation products [6].

According to Vogt et al. [12], three different pathways can be conceived during the hydrogenation of CO$_2$ to methane i.e., the carbide pathway through a CO intermediate, the formate pathway and the carboxyl pathway. The first two pathways have been observed for Ni-based catalysts through operando spectroscopic techniques (in-situ FTIR and ambient-pressure XPS), while the carboxyl pathway, though observed for Cu and Fe, is considered to be inactive for Ni-based catalysts [9,12]. Furthermore, catalyst supports can often play a major role in the methanation mechanism and the overall catalytic activity [13]. For example, Cárdenas-Arenas et al. [14] showed that oxygen species generated via CO$_2$ dissociation on Ni/CeO$_2$ catalysts could migrate throughout the ceria lattice and then be reduced at other sites, while the accumulation of formate intermediates at specific sites on Ni/Al$_2$O$_3$ catalysts delayed the chemisorption and activation of further CO$_2$ molecules. These different reaction routes caused by the oxygen ion mobility and lability of CeO$_2$-based supports could explain the greatly enhanced methanation activity of Ni catalysts supported on CeO$_2$ compared to other metal oxide supports [14–16].

The initial capture of CO$_2$ can be achieved by using liquids, such as aqueous amines, or solid materials, such as alkali and alkaline earth metal carbonates and oxides [17]. CaO solids promoted with different stabilizers are some of the most common CO$_2$ sorbents and the cyclical process that integrates CO$_2$ adsorption and desorption through CaO carbonization and calcination is often referred to as calcium looping [18]. Hydrogen from renewable sources can then be used to convert the captured CO$_2$. This whole process (CCU) is more energy efficient, since an exothermic CO$_2$ reduction step can provide the desired thermal energy for the endothermic desorption of captured CO$_2$ [5,19].

The combined CO$_2$ capture and conversion to methane can be realized either via the utilization of two different types of solids, namely one solid sorbent for the CO$_2$ capture and one methanation catalyst, or via the use of a single solid known as a dual-function material (DFM) that incorporates both the sorption and methanation functions [20]. The Farrauto group have been pioneers in this new and dynamic field, being the first to report a DFM consisting of CaO and Ru phases supported on a γ-Al$_2$O$_3$ support. The CaO and Ru phases functioned as CO$_2$ sorption and methanation active sites, respectively [19]. A recent review focusing exclusively on the combined CO$_2$ capture and conversion to methane has been published in early 2019 [20].

A common feature in the design of such DFMs is the incorporation of an alkali or alkaline earth metal oxide/carbonate phase (e.g., CaO, Na$_2$CO$_3$, K$_2$CO$_3$ and MgO) on a high surface area support (e.g., Al$_2$O$_3$ and ZrO$_2$) in order to be combined with adjacent catalytically active metal sites for CO$_2$ methanation [20,21]. Ru has been a favourite active metal due to its easier reducibility and coke-resistant propensity, but Ni is also studied in an attempt to curb the material's costs [22,23]. Various properties, such as the choice of the right support, the type of the CO$_2$ sorption phase and the appropriate sorbent loading, as well as the choice of the active metal or the right combination of metals, have an important role to play in enhancing the CO$_2$ sorption capacity and CH$_4$ yield of the designed material formulations [23–25].

Hereby we aim to summarize the most recent progress made in the field of alkali and alkaline earth metal promotion of the CO_2 methanation reaction and provide a comprehensive overview over the development of novel dual-function materials for the integrated capture and methanation of CO_2. The latter materials, by functioning as both catalysts and adsorbents towards the combined CO_2 capture and methanation, appear capable of improving the process and as a result have attracted intense interest in the last five years.

2. Alkali and Alkaline Earth Metals as Promoters of the CO_2 Methanation Reaction

There has been extensive effort in trying to achieve high catalytic activity, especially in the low-temperature region (ca. 100–250 °C), for the CO_2 methanation reaction. Rh and Ru are two of the most common precious metal catalysts studied in this reaction, since they achieve a substantial low-temperature activity and exhibit superior stability [26,27]. Ni-based catalysts, on the other hand, remain the favourite due to their low cost and large natural abundance, but they present some serious drawbacks, including inferior low-temperature activity when compared with Rh and Ru-based catalysts, as well as Ni nanoparticle sintering and coke formation [28,29]. Extensive research effort has been devoted in an attempt to enhance the low-temperature activity of Ni-based catalysts or decrease the loading of precious metal CO_2 methanation catalysts by introducing some kind of metal or metal oxide promoter [27].

Alkali and especially alkaline earth metal promotion of the CO_2 methanation reaction has been a quite popular route in recent years. These types of metals are cheap, abundant and can potentially promote the CO_2 methanation reaction by increasing support basicity and by introducing oxygen vacancies, thus favouring the initial CO_2 chemisorption [28,30,31], or even by strongly modifying the work function and thus the chemisoptive properties of the metal active phase [32]. Hereby, we categorize the different alkali and alkaline earth metal promoters starting from alkalimetals. Works that perform a screening of different promoters will be presented at first, followed by a categorization of the works focussing on a single metal promoter, depending on the type of metal used.

2.1. Alkalimetals (Li, Na, K and Cs)

2.1.1. Screenings of Various Alkalimetals

One of the few works reporting a promoting effect of various alkalimetals during the CO_2 methanation reaction was conducted by Petala et al. [33]. The authors employed quite a small loading of alkalimetal promoters (0.06–0.4 wt.% of Li, Na, K and Cs) by impregnating the corresponding alkali precursor salts on the TiO_2 support. A low (0.5 wt.%) and a high (5 wt.%) Ru loading was achieved via a subsequent impregnation step of $Ru(NO)(NO_3)_3$. The lower active metal loading resulted in a smaller Ru crystallite size. Interestingly, it was found that alkali addition had a greater impact on the catalyst with the low Ru loading (0.5 wt.%), in comparizon to that with the high Ru loading (5 wt.%), and an optimal Na loading of 0.2 wt.% was obtained for the former (i.e., 0.5 wt.% Ru/0.2 wt.% Na-TiO_2). These results agree with the general features of alkali promotion on several catalytic systems, which typically obey a volcano-type behavior with respect to the promoter/metal ratio; low promoter/metal ratios are inefficient to induce succesful promotion, high promoter/metal ratios lead to over-promotion (poisoning) [32]. The catalytic activity and CH_4 selectivity were promoted according to the following order with respect to the alkali identity: TiO_2 (unpromoted) < Li ≈ K < Cs < Na, as shown in Figure 1 [33]. In a continuation of this work, Panagiotopoulou [34] employed in-situ DRIFTS and transient-mass spectrometry in order to shed light on the reaction mechanism. Alkalimetal addition on the low Ru loading catalyst appeared to favour the formation of Ru-bonded carbonyl species (Ru_x-CO), which are key intermediates towards the production of CH_4.
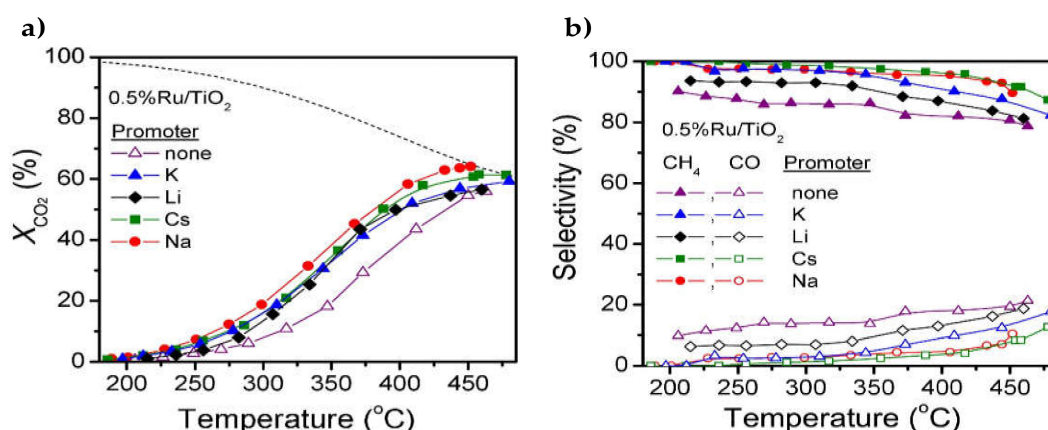
Figure 1. (**a**) Conversions of CO_2 and (**b**) selectivity toward CH_4 and CO as a function of reaction Table 0. Ru/X-TiO_2 catalysts of the same alkali loading (0.2 wt.%). Experimental conditions: mass of catalyst: 100 mg; particle diameter: $0.18 < d_p < 0.25$ mm; feed composition: 5% CO_2, 20% H_2 (balance He); total flow rate: 150 cm^3 min^{-1}. Reproduced with permission from ref. [33]. Copyright 2018 Elsevier.

The impact of alkalimetal addition on a Ru-based catalyst towards the methanation of CO_2 was also studied by Cimino et al. [35] in a recent study. In this case, a higher alkali promoter loading was chosen and the impregnation of the alkali precursor salts took place mostly after the impregnation of the Ru active metal. All alkali modified catalysts, except the one modified with $LiNO_3$, exhibited lower CO_2 conversions and CH_4 selectivities compared to the unmodified 1% Ru/Al_2O_3 one. The lower catalytic activity was attributed to the coverage of some Ru active sites, while Li could promote the Ru-based catalyst activity by forming Li-aluminate spinel-type phases with the Al_2O_3 support. The $LiNO_3$ and $NaNO_3$ promoted materials were also tested for cyclic CO_2 capture and methanation and the results will be further discussed in the second part of this review.

Liang et al. [36] and Zhang et al. [37] studied the effect of K and Na modification (amongst other metals) on Ni/Al_2O_3 and Co/Al_2O_3 catalysts, as well as the alteration of the CO_2 methanation mechanism via in-situ DRIFTS. In the first study [36], a total of 16 different metal additives were first impregnated on a γ-Al_2O_3 support, followed by a subsequent impregnation of Ni. Na and K additives gravely impacted the physicochemical properties of the catalysts, leading to lower activity. The lower catalytic activity of the K-modified catalyst was attributed to the increased population of H_2CO^* intermediates. In the second study [37], the modification of the alumina support in Co/Al_2O_3 by K, Na and Mg led to the formation of Al(OH)$_3$ and spinel-type structures. The addition of Na and K followed by the increase in support alkalinity appeared to stir the reaction towards $HCOO^*$ and CO_3^{2-} intermediates, lowering the catalytic activity and CH_4 selectivity, as well as favouring coke formation. The promotion of the CO_2 chemisorption by alkalimetal addition did not appear to correlate with the catalytic activity.

In regards to the electrocatalytic CO_2 methanation, the Vayenas group employed the electrochemical promotion of catalysis (EPOC) concept, an effective in-situ method of catalyst promotion, also known as non-faradaic electrochemical modification of catalytic activity (NEMCA) [32,38] to enhance CO_2 methanation performance of a Ru electrocatalyst [39,40]. Taking advantage of the high potential of the method, the authors comparatively investigated a variety of electropositive or electronegative promoters, namely Na^+, K^+, H^+ and O^{2-}. They found that in all cases, increasing catalyst work function (induced by the promoters) enhances the methanation rate and selectivity. In the case of the present interest (alkali promotion), Na^+ and K^+ supply to Ru surface caused a remarkable promotion of the methanation rate, which was found to pass through a maximum upon increasing alkali loading (volcano-type promotion). This result is in qualitative agreement with the typical features of alkali-promotion [32] and with the aforementioned results of Petala and Panagiotopoulou on CO_2

methanation over traditional supported Ru catalysts upon varying Na-loading by an impregnation method [33].

2.1.2. Sodium (Na)

Among the works focusing on the support modification with Na, Le et al. [41] investigated the CO_2 methanation reaction over Ni catalysts supported on Na (0.1–1 wt.%) doped SiO_2 and CeO_2 supports. Na was incorporated (via impregmation) in the previously made 33% Ni/SiO_2 and 13% Ni/CeO_2 catalysts in a second impregnation step using a $NaNO_3$ precursor. The available active metal surface area was shown to decrease upon Na addition, following H_2 chemisorption experiments. Subsequently, CO_2 conversion decreased upon Na modification of the initially highly active Ni/CeO_2 catalyst, while the increase of the amount of moderately strong basic sites and CO_2 chemisorption sites following the incorporation of Na in Ni/SiO_2 appeared to offset the negative effect caused by the decrease of the catalytically active surface area.

Moreover, Beierlein et al. [42] employed various preparation methods in order to prepare Ni/Al_2O_3 catalysts with high Ni loadings (14–88 wt.% Ni). The primary focus of their work was to establish a linear correlation between the surface area of the active metal (Ni) and the CO_2 conversion, arguing that CO_2 methanation over highly loaded Ni/Al_2O_3 catalysts is a structure-insensitive reaction. Two of the preparation methods applied, namely deposition precipitation and coprecipitation, required the use of large quantities of NaOH and Na_2CO_3 reagents, thus introducing a relatively high content of Na on the final catalysts. A high Na content was shown to decrease CH_4 selectivity, while boosting CO production. This behaviour was attributed to the lower hydrogen coverage of the active metal and the hindrance of the H-assisted CO dissociation, a key intermediate step (also reported to be the rate determining step [9]) during the conversion of CO_2 to CH_4.

2.1.3. Pottasium (K)

Pottasium-doping of the catalyst support has been performed by various groups with most of them reporting a negative effect on the CO_2 methanation. Büchel et al. [43] studied the CO_2 hydrogenation over K- and Ba-modified 1% Rh/Al_2O_3 catalysts prepared by flame spray pyrolysis. The K-modified catalyst produced only CO over the entire temperature range. This extreme CO selectivity over CH_4 was attributed to a weak interaction of CO with the catalyst, as shown during CO chemisorption experiments. This could cause the intermediate CO species to desorb, rather than be further hydrogenated into CH_4. Iloy et al. [44] further studied the modification of 15% Co/SiO_2 with 1–5 wt.% K. K-dopant was shown to enhance CO_2 chemisorption, but favour CO selectivity and C–C coupling along with chain growth reactions. For the production of C_{2+} hydrocarbons, 1 wt.% K appeared to be optimal, while a higher potassium loading favoured CO as a main product.

Modification of the Al_2O_3 support with a KOH strong base was performed by Zhang et al. [45] and the reaction intermediates were followed via in-situ DRIFTS. KOH was first dissolved in d-H_2O and then introduced into the Al_2O_3 support, while Ni was impregnated during a second step. KOH addition led to a dramatic decrease of the Al_2O_3 surface area and after calcination, K_2CO_3 and K_2O phases were also detected. The introduction of the strong KOH base led to the increased presence of adsorbed formate intermediates during CO_2 hydrogenation, which was validated via in-situ DRIFTS (Figure 2) [45]. This strong interaction with the formate intermediate species apparently did not allow for their further hydrogenation to CH_4 and instead led to a high CO selectivity. The Ni-KOH/Al_2O_3 catalysts, on the other hand, could be considered as more suitable candidates for the RWGS reaction and the steam reforming of acetic acid, in an antithesis to other works:
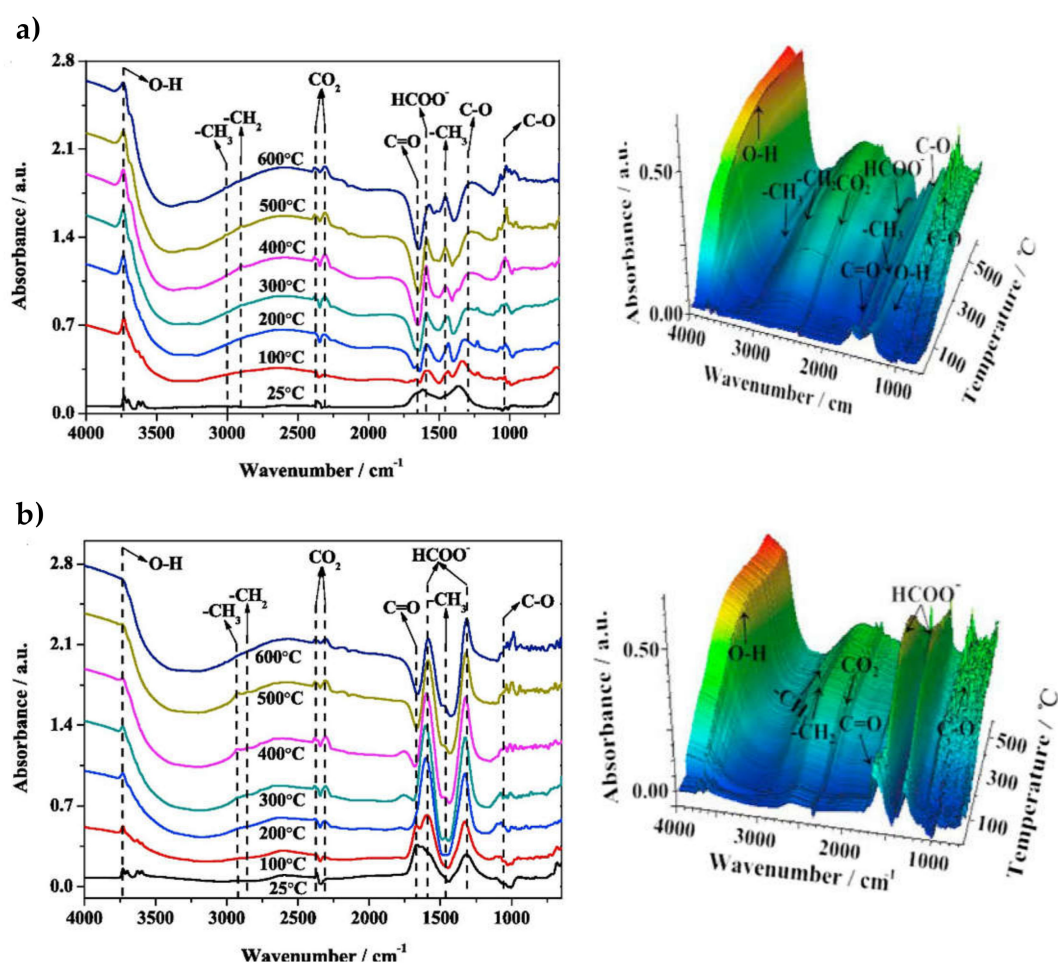
Figure 2. In-situ DRIFTS characterization for the CO_2 methanation over Ni/Al_2O_3 and $Ni-KOH/Al_2O_3$ catalysts. (**a**): Ni/Al_2O_3, (**b**): $Ni-KOH/Al_2O_3$. Reaction conditions: CO_2/H_2 = 1/4; (CO_2 = 10 mL/min; H_2 = 40 mL/min; N_2 = 50 mL/min). Reproduced with permission from ref. [45]. Copyright 2018 Elsevier.

He et al. [46] reported a promoting effect of KOH addition towards higher CO_2 conversions and CH_4 selectivities, when impregnated on a Ni-Al hydrotalcite precursor. This was attributed to the introduction of new strong basic sites in the support. The different behaviour in this case could be likely due to the small loading of the KOH base (0.3 wt.%), similarly to the work of Petala et al. [33]. This also demonstrates the key role of the alkali promoter/active metal ratio in alkali promotion efforts and the nessecity of a thorough screnning for the determination of the optimal alkali promoter loading for each specific catalytic system, alkali indentity and reaction conditions used [47,48].

Another interesting study that includes an in-situ KOH modification of a Ni/SiO_2 methanation catalyst has been conducted by Vogt et al. [49]. The authors first created a setup that produced hydrogen through solar driven H_2O electrolysis from a KOH-based alkaline electrolyzer. Produced H_2 was then transferred downstream to a methanation unit that contained a Ni/SiO_2 methanation catalyst. During operation, KOH aerosols were transferred to the methanation reactor and part of them was deposited on the Ni-based catalysts. Interestingly, this in-situ alkali modification promoted the Ni/SiO_2 methanation catalyst, whereas a similar ex-situ 0.6 wt.% K addition via a common KOH impregnation resulted to catalyst deactivation.

$LaNiO_3$-based perovskite oxides can serve as catalyst precursors for the preparation of Ni/La_2O_3 catalysts following a reductive pretreatment. The fine and well-dispersed Ni nanoparticles formed following the perovskite lattice decomposition retain a strong interaction with the La_2O_3 support and are expected to exhibit a different behaviour compared to the Ni/La_2O_3 catalysts prepared via

a mere impregnation step [50]. Tsounis et al. [51] presented a way to tune the product selectivity of $LaNiO_3$-based perovskites during CO_2 hydrogenation, via partially substituting La on the perovskite A-site with K. KNO_3 was mixed together with La and Ni nitrates during the perovskite citrate sol-gel synthesis, in order to prepare $La_{1-x}K_xNiO_3$ precursors. Following reduction, the catalysts exhibited a drastically different behaviour during CO_2 hydrogenation depending on the amount of K-doping. The K-free catalyst had a high CO_2 conversion and an almost complete selectivity towards CH_4, while with increased amounts of K-substitution CO_2 conversion gradually decreased and CO selectivity spiked (Figure 3). A possible explanation given was that easy-to-desorb CO intermediates were formed after K-doping and they in turn stirred the reaction towards the RWGS route.
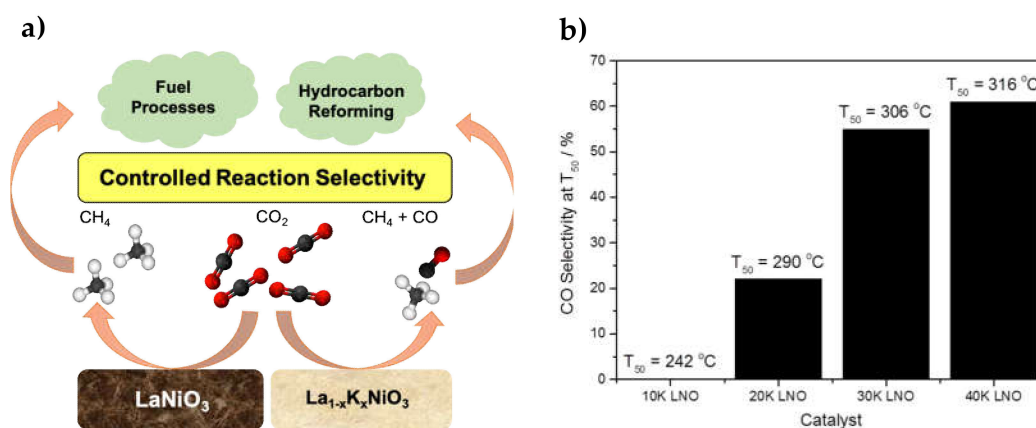

Figure 3. (a) CO_2 hydrogenation product selectivity for the catalysts derived from $LaNiO_3$ and K-substituted ($La_{1-x}K_xNiO_3$) perovskites; (b) rising CO selectivity towards the RWGS at $T_{50\%}$ for the catalysts containing increased amounts of K. Reproduced with permission from ref. [51]. Copyright 2020 MDPI.

2.2. Alkaline Earth Metals (Mg, Ca, Sr and Ba)

2.2.1. Screenings of Various Alkaline Earth Metals

In the works discussed previously, some alkaline earth dopants were also used and compared with the effect caused by the doping with alkalimetals. Zhang et al. [37] concluded that the effect of Mg and Ca addition on Co/Al_2O_3 was less pronounced compared with Na and K and that, although the activity of the modified catalysts was inferior to Co/Al_2O_3, alkaline earth metal doping still provided a benefit by preventing Co nanoparticle sintering during prolonged exposure under reaction conditions. Liang et al. [36] also mentions that 5% Mg and Ca doping on Ni/Al_2O_3 led to a slight increase in support alkalinity, but did not appear to benefit the methanation activity.

Guo et al. [52] were among the first to conduct a comparative study on the impact of alkaline earth metal addition on Ni/SiO_2 catalysts. During the catalyst preparation, alkaline earth metal nitrates were first impregnated on the SiO_2 support, followed by wet impregnation of the Ni active phase. The authors reported that MgO had a negative effect on the catalytic activity, while CaO did not have a pronounced effect. The heavier alkaline earth metal oxides SrO and BaO led to better results, both enhancing the catalytic activity. SrO was shown to be the most suitable additive by providing the highest promotion of the CO_2 methanation reaction and by increasing the stability of the modified catalyst.

Liang et al. [53] studied the modification of Ni/Al_2O_3 catalysts with alkaline earths for the CO_2 methanation reaction and reported similar results. The catalysts were also prepared via subsequent impregnation of alkaline earth metal nitrates and then nickel nitrate on the support. The lighter alkaline earth metals Mg and Ca were found to promote the formation of carbonate intermediates and the CO selectivity, while the heavier alkaline earth metals Sr and Ba were the ones being beneficial for the

CH$_4$ yield by promoting the formation of *CO and H$_2$CO* intermediates. Another important feature, namely the generation of oxygen vacancies upon Sr-addition, appeared to play a major role via the creation of Lewis basic sites for the adsorption and activation of CO$_2$.

Ni/CeO$_2$ catalysts are among the most active for CO$_2$ methanation and are a main research focus. CeO$_2$ has a high oxygen storage capacity (OSC) that, together with its redox properties due to the Ce^{4+}/Ce^{3+} redox couple, promotes the stability of the active metal particles and suppresses the formation of coke. Furthermore, CeO$_2$ facilitates a strong interaction with the supported metal phase [54,55]. Liu et al. [30] conducted a comprehensive study, where they doped the CeO$_2$ support of Ni/CeO$_2$ catalysts with various alkaline earth metals, with the aim to further enhance their low-temperature catalytic activity. Alkaline earth metal nitrates were introduced during the citrate sol-gel synthesis of the CeO$_2$ support with a molar ratio of 1/9, compared with Ce(NO$_3$)$_3$·6H$_2$O. Mg^{2+} and Ca^{2+} appeared to fully dissolve into the CeO$_2$ lattice, while SrCO$_3$ and BaCO$_3$ secondary phases were detected in the other two samples. The Ca-doped catalyst induced the highest promotion effect, measured via the CO$_2$ conversion and turnover frequency (TOF) increase at low temperatures, with the Sr-doped one being second-to-best. The higher turnover frequency could be linearly correlated with two related factors, namely the increase in the population of oxygen vacancies (Ce^{3+}/(Ce^{3+} + Ce^{4+}) molar ratio) and moderate alkaline sites (200–450 °C peaks in the CO$_2$-TPD profiles), as shown in Figure 4.
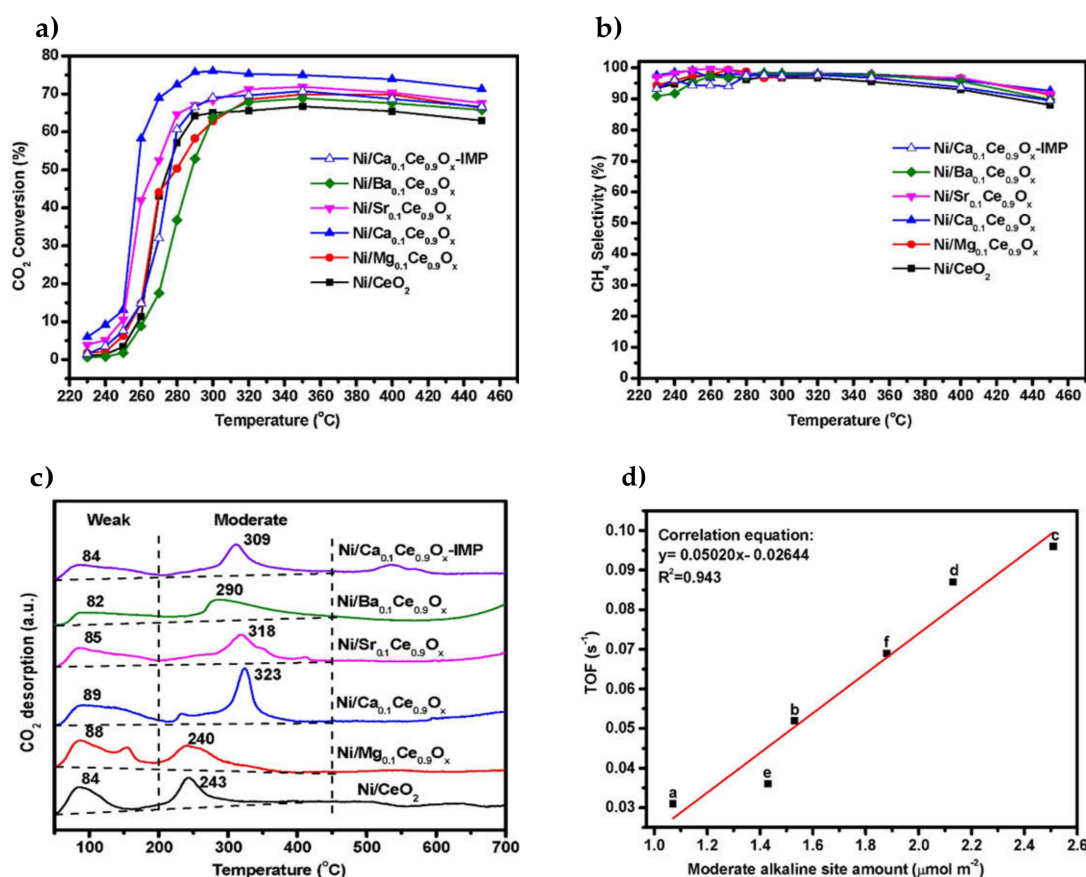
Figure 4. CO$_2$ conversion (**a**) and CH$_4$ selectivity (**b**) of the Ni/M$_{0.1}$Ce$_{0.9}$O$_x$ catalysts; WHSV = 36,000 mL h^{-1} g^{-1}. (**c**) CO$_2$ desorption profiles of the Ni/M$_{0.1}$Ce$_{0.9}$O$_x$ catalysts and (**d**) Linear relationship between the TOF values at 250 °C and the amount of surface moderate alkaline sites on the Ni/M$_{0.1}$Ce$_{0.9}$O$_x$ catalysts. a. Ni/CeO$_2$; b. Ni/Mg$_{0.1}$Ce$_{0.9}$O$_x$; c. Ni/Ca$_{0.1}$Ce$_{0.9}$O$_x$; d. Ni/Sr$_{0.1}$Ce$_{0.9}$O$_x$; e. Ni/Ba$_{0.1}$Ce$_{0.9}$O$_x$; f. Ni/Ca$_{0.1}$Ce$_{0.9}$O$_x$-IMP. Reproduced with permission from ref. [30]. Copyright 2020 Elsevier.

The studies discussed up to this point, which focused on the screening of different alkaline earth metals as dopants, appear to provide conflicting conclusions on their effect, since some of them

report enhancement of the CO_2 methanation activity, while others a suppression of it (for Mg and Ca). One must take into account that these works differ on the type of support, the alkaline earth metal loading and the preparation procedure. Notably, almost all works focusing on a single alkaline earth metal additive, especially concerning Mg and Ca doping, report a promoting effect for the CO_2 methanation. Generally, this promotion is attributed to a better active metal dispersion, as well as to the generation of surface oxygen vacancies and the enhancement of support alkalinity, factors that substantially favour the initial chemisorption and activation of CO_2.

2.2.2. Magnesium (Mg)

Mg in the form of MgO has been studied as a type of support during the CO_2 methanation reaction. However, Ni/MgO catalysts have been shown to lack the activity of other Ni catalysts supported, for example, on TiO_2, Al_2O_3 and CeO_2 [15]. The CO_2 methanation mechanism over Ni/MgO has been reported to proceed via a H_2COO* intermediate and to follow the formate route, due to the strong metal-support interaction (SMSI) between the Ni nanoparticles and the MgO support [56]. Ni/MgO catalysts encapsulated by a SiO_2 shell were prepared by Li et al. [57] via chemical co-precipitation and a modified Stöber method, followed by in-situ reduction of the initial SiO_2 encapsulated NiO-MgO solid solution. Interestingly, it was found that the confinement induced by the SiO_2 shell helped to control the size of Ni nanoparticles, whereas the MgO phase also contributed to the improved Ni dispersion.

Besides its function as a catalyst support, MgO has also been thoroughly studied as a promoter for the CO_2 methanation reaction in an attempt to improve the dispersion of the active metal phase and enhance the support basicity. Park et al. [58,59] reported a bifunctional mechanism of CO_2 methanation over a Pd-MgO/SiO_2 catalyst. The addition of MgO in Pd/SiO_2 led to improved catalytic activity and CH_4 selectivity. A mechanism was proposed where MgO and Pd phases functioned as CO_2 and H_2 sorption active sites, respectively. The adsorbed hydrogen atoms on the Pd surface were then proposed to spillover to Mg carbonates, hydrogenating the CO_2-adsorbed phases and forming the CH_4 final product. This bifunctional character of CO_2 methanation reaction that requires the presence of a catalyst componente capable of activating the CO_2 (Supporting Material: even the commonly considered "inert" Al_2O_3 acts in this way; support doping is often used for further enhancing this role), and a metallic component typically active in H_2 dissociation has been well established in the literature [60–62].

Guo et al. [63] prepared Ni/SiO_2 catalysts with different MgO loadings and with two different preparation methods, namely co-impregnation and sequential impregnation. Co-impregnation was shown to be superior to sequential impregnation and 1% MgO loading to be sufficient for the reaction promotion, whereas a higher MgO content risked masking some of the Ni active sites. The promotion was reportedly achieved via the enhancement of Ni dispersion and via Ni particle sintering prevention. The beneficial effect of MgO in the Ni nanoparticle dispersion was also reported by Tan et al. [64]. Ni and Mg nitrates were co-impregnated on a ZrO_2 support with the simultaneous addition of citric acid and glycol during the impregnation step, applying the citric complexing method. An optimal Mg/Ni molar ratio of 0.25 led to the desired Ni nanoparticle confinement and resistance to sintering and coke formation. Moreover, Xu et al. [65] included Mg in the synthesis of ordered mesoporous Ni/Al_2O_3 catalysts prepared via evaporation-induced self-assembly (EISA). Mg increased the surface basicity of the catalysts, thereby facilitating the chemisorption and activation of CO_2. The optimized Mg content of 5% and the confinement created by the mesoporous alumina structure provided significant advantages for the employment of these materials in the CO_2 methanation reaction.

Further studies include the promotion of Ni-based catalysts supported on coconut shell carbon (CSC) [66] and MCM-41 [67] with Mg, as well as the Mg-modification of catalysts comprised of Ni supported on ultrastable Y (USY) and MFI (Mobil-type five) nanosponge zeolites [68,69]. All these studies reported an improvement of the CO_2 methanation catalytic performance. Additionally, a second promoter could also be introduced together with Mg to investigate co-promotion effects [70,71]. La-promoted Ni/MgO-Al_2O_3 catalysts showed improved low-temperature activity via the increase in

the population of moderately strong basic sites [60], while Mg and Mn co-promoted Ni/α-Al$_2$O$_3$ catalysts were shown to be superior compared to the ones prepared with the use of a single promoter [71].

Finally, Mg has been indicated as a suitable promoter for Fe catalysts during CO$_2$ methanation [72]. Fe catalysts, commonly known to be active during the Fischer–Tropsch synthesis, could also be viable candidates for the CO$_2$ hydrogenation into CH$_4$ under high pressure, after the incorporation of a suitable promoter [73]. Baysal et al. [72] incorporated a series of 15 different promoters on a commercial α-Fe$_2$O$_3$ powder via incipient wetness. Improved CO$_2$ adsorption over the Mg-modified Fe catalyst led to highly active Fe carbides, bulk carbon moieties and an overall improved CO$_2$ methanation performance.

2.2.3. Calcium (Ca)

Ca is also one of the favourite promoters for the CO$_2$ methanation reaction, with its main functions being the increase in the population of surface basic sites and the alteration of support defect chemistry by introducing oxygen vacancies. Similarly to the Mg doping of Ni-based catalysts supported on ordered mesoporous alumina [65], Ca was also employed as a basic modifier by Xu et al. [74]. Ca(NO$_3$)$_2$·4H$_2$O was introduced during the evaporation-induced self-assembly (EISA) catalyst synthesis. The surface alkalinity was greatly increased upon Ca-doping and that led to an enhancement of CO$_2$ chemisorption and a lowering of the activation energy for CO$_2$ methanation. The spike in the population of new strong alkaline sites was confirmed by CO$_2$-TPD. The catalytic activity was the highest, when the Ca/Al molar ratio was fixed at 8%, with a roughly 4 times CO$_2$ conversion increase at low temperatures (250 °C).

Liu et al. [75] tried to further optimize these types of catalysts by an additional introduction of 1% Ru. The 10N1R2C-OMA or 1% Ru, 10% Ni, 2% CaO/Al$_2$O$_3$ (ordered mesoporous alumina) catalyst aimed at combining the beneficial effects of: (a) the nanoparticle confinement inside an ordered mesoporous alumina framework, (b) the increase of surface basicity and CO$_2$ chemisorption using a CaO promoter and (c) the introduction of 1% noble metal Ru, forming a bimetallic NiRu phase and creating a synergy between the two catalytically active metals. A step increase in the CO$_2$ conversion and CH$_4$ selectivity was reported following the subsequent introduction of each modifier. Furthermore, the ordered mesoporous structure and the fine dispersion of the active metal phase were retained in the spent catalysts, highlighting their superior stability. The methanation performance of the prepared catalysts, as well as the stability test for the 10N1R2C-OMA one, are shown in Figure 5.
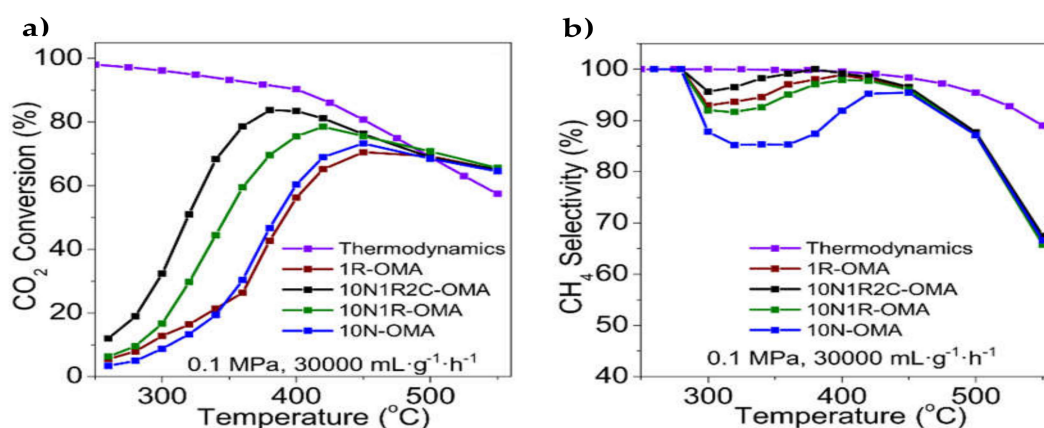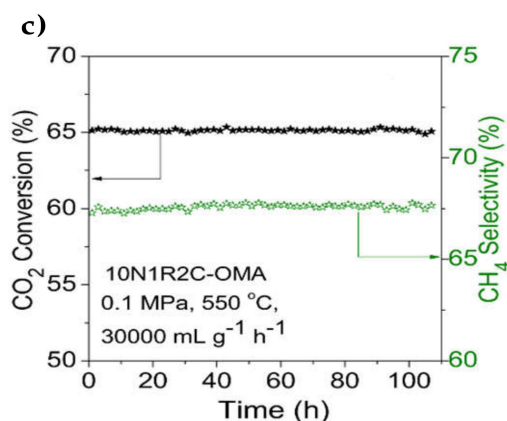

Figure 5. *Cont.*

c)

Figure 5. Catalytic properties of the prepared catalysts: (**a**) CO_2 conversion and (**b**) CH_4 selectivity; (**c**) lifetime test of the 10N1R2C-OMA catalyst. Reproduced with permission from ref. [75]. Copyright 2018 Elsevier.

Furthermore, Do et al. [76] reported a promoting effect of CaO addition on a bimetallic PtNi/Al_2O_3 catalyst during methanation of a CO_2-rich gas, while the group of Chu also published a a number of works focussing on the introduction of Ca-dopant as a promoter for the methanation of CO_2 [77–79]. A 20% CaO addition on 15% Ni/Al_2O_3 was reported to modify the interaction between Ni and Al_2O_3 and inhibit the incorporation of Ni into the alumina structure [77], while Ca addition on carbon supported Ni catalysts (carbon nanotubes [78] and activated carbon [79]) also appeared to be beneficial by increasing Ni reducibility and by limiting the growth of the Ni nanoparticles.

Ca^{2+} cations are soluble into the crystalline lattice of ZrO_2 and the corresponding solid solution is commonly known as calcia stabilized zirconia (CSZ). Oxygen vacancies (V_o^2) are created in order to compensate for the negatively charged Ca-induced substitutional impurities ($Ca_{Zr}^{2'}$), thereby enhancing the material's ionic conductivity and altering its defect chemistry [80]. Takano et al. [81] impregnated Ni and Ca nitrates on ZrO_2 and studied the effect of Ca/(Zr + Ca) molar ratio on the CO_2 methanation activity. The authors argued that the presence of medium-strength basic sites caused by the Ca-induced oxygen vacancies could facilitate CO_2 chemisorption, which then further reacted with atomic hydrogen adsorbed on Ni adjacent sites. An optimized Ca/(Zr + Ca) molar ratio between 16.7% and 20% was shown to maximize the population of oxygen vacancies, while preventing the formation of undesirable Ca-rich and $CaZrO_3$ phases. More recently, Everett et al. [82] showed that a small amount of Ca^{2+} substitution (0.7 wt.%) in the lattice of ZrO_2 generated pairs of oxygen vacancies and coordinately unsaturated sites (cus). They concluded that these pairs could facilitate the C-O bond scission on adsorbed intermediate CO, reportedly the rate determining step during CO_2 methanation.

Finally, perovskite oxide titanates containing Ca have been also used in the CO_2 methanation reaction. Jia et al. [83] employed a common perovskite oxide that is also found as a natural mineral, $CaTiO_3$, as a catalyst support and compared it with γ-Al_2O_3. The 10% Ni/$CaTiO_3$ catalyst exhibited CO and CO_2 methanation activity superior to 10% Ni/Al_2O_3, due to the perovskite oxide's exceptional stability, increased support basicity and the limited interaction between Ni particles and the $CaTiO_3$ support. Do et al. [84] used Ca as a promoter in order to substitute part of the A-site cations in the $NiTiO_3$ lattice and the whole perovskite was loaded on γ-Al_2O_3. They performed extensive characterizations on the composite materials and concluded that upon 5% molar substitution of Ni^{2+} with Ca^{2+}, the catalytic activity could be maximized. Ca-addition promoted the formation of oxygen vacancies in close proximity to Ni active phases and thereby the CO_2 chemisorption. The proposed reaction mechanism, as summarized in Figure 6, involved a combination of the CO and formate routes. The initial CO_2 adsorption and hydrogenation steps resulted into formate species, which in turn formed adsorbed CO. The carbonyl species were then further reduced to form other hydrogenated intermediates, with CH_4 being the final product.
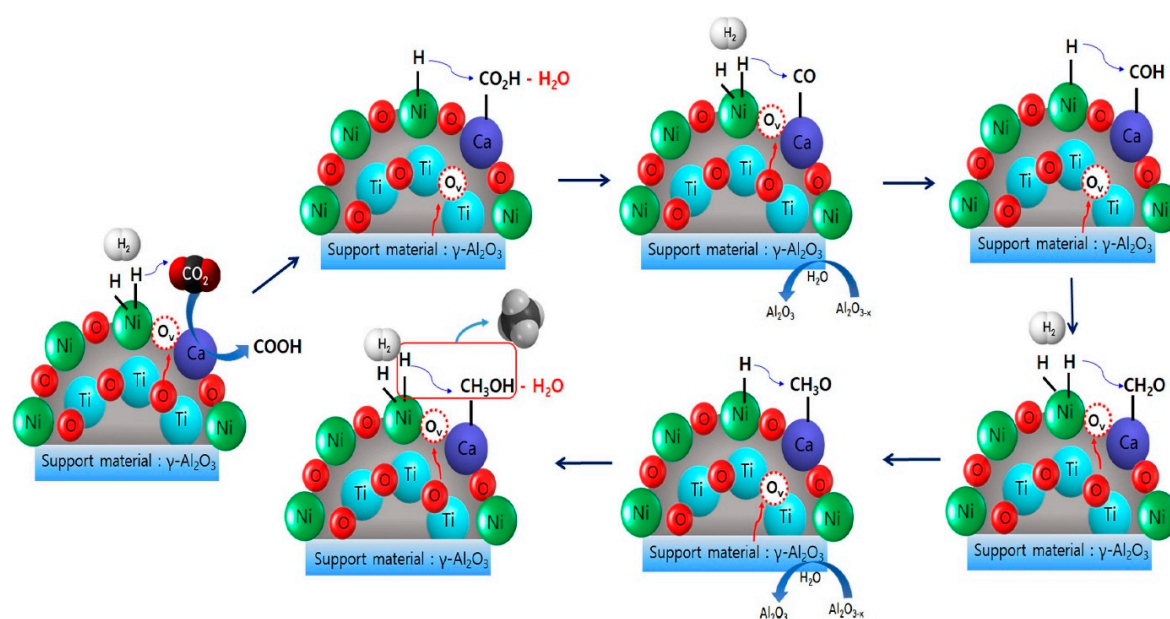
Figure 6. Plausible mechanism for CO_2 methanation over the Ca-NiTiO$_3$/γ-Al$_2$O$_3$ catalysts. Reproduced with permission from ref. [84]. Copyright 2020 Elsevier.

2.2.4. Strontium (Sr) and Barium (Ba)

Despite the fact that the works dealing with the screenings of different alkaline earth metal promoters report a quite beneficial contribution upon Sr and Ba addition [30,52,53], little further research has been conducted on the individual promotion of either of these heavier elements, especially when compared to their lighter alkaline earth metal counterparts. Toemen et al. [85] modified a Ru/Mn/Al$_2$O$_3$ catalyst with Sr and Ce. The Sr-modified catalyst initially adsorbed increased amounts of CO_2 as monodentate carbonates, which in turn formed bridged bidentate carbonates before being further hydrogenated. The enhanced catalytic activity of the Sr-doped catalyst was, however, overshadowed by the Ce-doped one, where the methanation reaction followed a different mechanism.

Steiger et al. [86] prepared La$_{1-x}$Sr$_x$Fe$_{0.8}$Ni$_{0.2}$O$_3$ perovskite oxides with increasing amounts of A-site Sr substitution. Pre-reduction of the initial perovskite caused the lattice Ni to be exsolved on the perovskite surface in the form of fine and well-dispersed Ni nanoparticles that exhibited strong interaction with the perovskite support. The amount of exsolved Ni, as well as the size and dispersion of the Ni nanoparticles, could be tailored by altering the A-site perovskite composition. La substitution on the A-site by Sr caused a destabilization of the perovskite lattice and an increase in the amount and population of exsolved Ni nanoparticles. This in turn promoted the CO_2 methanation reaction by increasing the CH$_4$ yield, though a possible modification of the surface chemistry due to the increased presence of Sr could also affect the reaction.

Regarding Ba, it was mentioned in a previously discussed work [43] that K-modified 1% Rh/Al$_2$O$_3$ was highly selective towards CO. The authors also prepared a Ba-modified Rh/Al$_2$O$_3$ catalyst, whose catalytic performance was similar to the unpromoted Rh/Al$_2$O$_3$ one. However, the CH$_4$ yield was lower, especially at lower temperatures, and the enhanced CO_2 affinity due to the Ba-addition did not benefit the overall methanation activity. The results appear to contrast the findings of previously discussed works [52,53] that report a promoting role of Ba for the CO_2 methanation reaction, probably as a result of different types of catalysts, preparation methods, reaction conditions and Ba loadings used.

2.3. Hydrotalcite-Derived and Zeolite Supported Catalysts

Besides commonly used supports such as Al$_2$O$_3$, ZrO$_2$, SiO$_2$ and TiO$_2$, MgO-Al$_2$O$_3$ mixed oxides derived from Mg-containing hydrotalcites, as well as zeolites, have also become popular

CO_2 methanation catalyst supports in recent years. Hydrotalcites, or layered double hydroxides, with Ni^{2+} and Mg^{2+} as divalent cations can be calcined and reduced at high temperatures in order to produce active catalysts that consist of Ni nanoparticles supported on a $MgO-Al_2O_3$ mixed oxide. Mg^{2+} presence in the initial hydrotalcite facilitates the creation of alkaline sites on the support that favour CO_2 chemisorption and activation. Zeolites can also be impregnated with an active metal phase (e.g., Ni and Rh) to be used as methanation catalysts. These types of catalysts have gained increased traction recently and two review articles have been published summarizing the progress made [87,88]. Since an Mg component is mostly present in hydrotalcite-derived catalysts and alkali, as well as alkaline earth metals, serve as compensating cations in zeolites, we will provide here a brief overview on the influence that these two parameters exert on the CO_2 methanation activity.

2.3.1. Hydrotalcite-Derived Catalysts

Hydrotalcite materials, also known as layered double hydroxides, have the general formula of $[M_{1-x}^{2+}M_x^{3+}(OH)_2](A^{n-})_{x/n} \cdot mH_2O$ with M representing divalent and trivalent metals and A being an anion. Mg^{2+} and Ni^{2+} can serve as divalent cations, while Al^{3+} is a common trivalent cation. Upon calcination and reduction, supported Ni catalysts are obtained with high activity and selectivity for specific catalytic reactions [87]. Bette et al. [89] claimed to be the first to present an active CO_2 methanation catalyst derived from a hydrotalcite precursor ($Ni_{0.5}Mg_{0.17}Al_{0.33}(OH)_2(CO_3)_{0.17} \cdot mH_2O$) synthesized via the coprecipitation method. The resulting catalyst consisted of a high Ni loading (59 wt.%) supported on a spinel-type $(Mg,Al)O_x$ mixed oxide and exhibited stable catalytic performance, as well as Ni particle sintering and coking resistance.

The cooperation between the Ni catalytically active phase and the MgO alkaline phase in hydrotalcite-derived catalysts has been studied by Liu et al. [90]. The authors varied the Ni^{2+}/Mg^{2+} molar ratio during the coprecipitation synthesis, while the ratio between trivalent (Al^{3+}) and divalent (Mg^{2+} and Ni^{2+}) cations remained constant. After calcination and reduction, the formed Ni nanoparticles were well-dispersed over the $MgO-Al_2O_3$ support with an average crystallite size of about 2.5 nm. Two types of basic sites were observed upon CO_2-TPD, namely weak basic sites for CO_2 adsorbed on Al_2O_3 phase and moderately strong basic sites for CO_2 adsorbed on MgO phase. Regarding the catalytic performance for CO_2 methanation, the hydrotalcite-derived catalysts presented far superior low-temperature CO_2 conversion compared with other Ni-based catalysts supported on Al_2O_3, MgO and carbon nanotubes (CNTs) (Figure 7a). Moreover, a linear correlation could be derived between TOF_{Ni} values and the amount of moderately strong basic sites on the support (Figure 7c). The reaction mechanism proposed involved a CO_2 activation step by the support basic sites to carbonate/hydrocarbonate species and an H_2 dissociation step on the Ni metallic sites. The interplay between these two phases facilitated the excellent low-temperature activity towards CO_2 methanation.
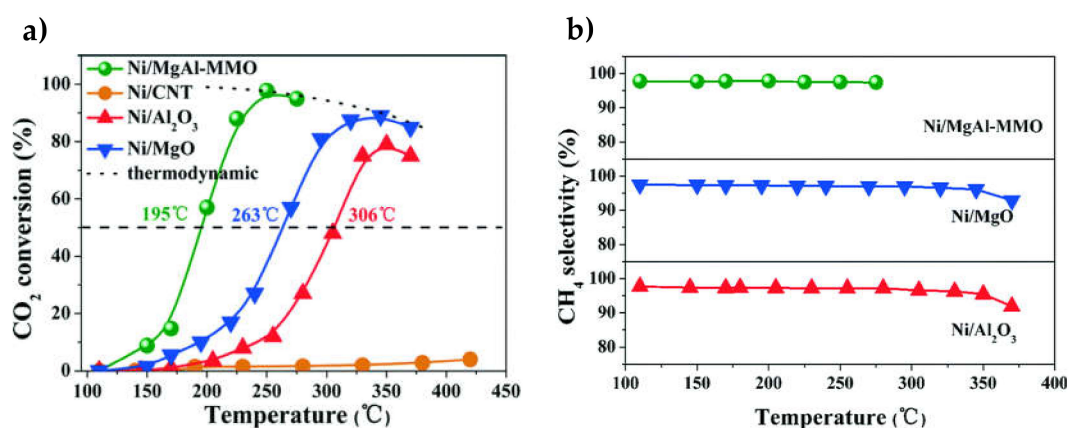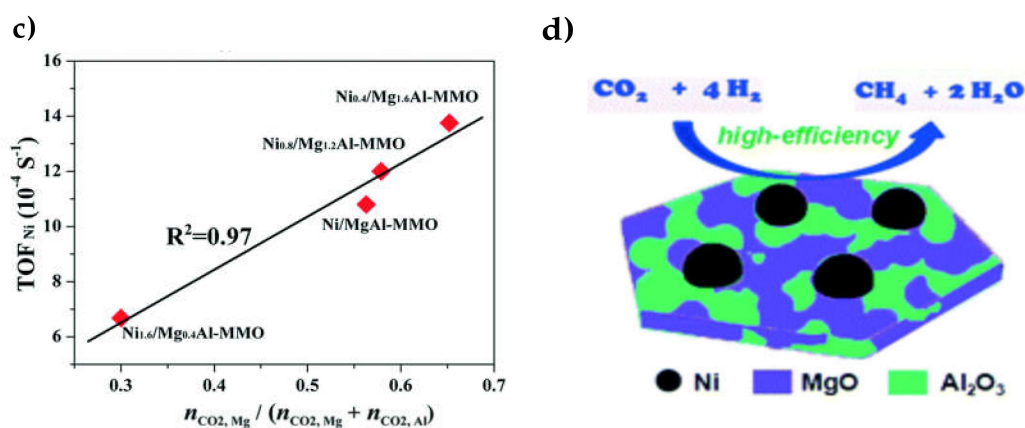

Figure 7. *Cont.*

Figure 7. (**a**) CO_2 methanation at steady state as a function of reaction temperature over the as-prepared Ni/MgAl-MMO, Ni/CNT, Ni/Al$_2$O$_3$ and Ni/MgO catalysts (GHSV: 2400 h^{-1}). (**b**) The corresponding selectivity toward CH$_4$ as a function of reaction temperature. (**c**) Relationship between the TOF$_{Ni}$ values and the concentration of alkaline sites in the Ni$_x$/Mg$_{2-x}$Al-MMO catalyst and (**d**) CO_2 methanation over the hydrotalcite-derived catalysts that consist of Ni nanoparticles finely dispersed over a MgO-Al$_2$O$_3$ mixed oxide support (Ni/MgAl-MMO). Reproduced with permission from ref. [90]. Copyright 2016 Royal Society of Chemistry.

Further works report on the influence of other parameters, as well as on the incorporation of further promoters and metals. Ren et al. [91] changed some variables during the hydrotalcite coprecipitation synthesis that led to platelet-like and rosette-like support structures and emphasised on the effect of support morphology and metal-support interaction over the CO_2 methanation performance. Wierzbicki et al. [92,93] introduced La during the hydrotalcite preparation to further promote the support alkalinity and CO_2 chemisorption, as well as the interaction between the Ni phase and the hydrotalcite-derived support. Additionally, bimetallic catalysts were prepared by Martins et al. [94], with Ru being impregnated over the initial Ni-Mg-Al hydrotalcites, while Mebrahtu et al. [95] varied the amount of added Fe during the hydrotalcite synthesis. The intimate mixing of the Ni^{2+} and Fe^{3+} metal cations led to the formation of NiFe alloys after reduction and the alloy composition could be correlated with the catalytic performance [95]. We can thereby conclude that hydrotalcite precursors offer a unique possibility to tailor the catalyst composition and morphology, as well as examine the influence of various different factors towards enhancing the CO_2 methanation activity and stability.

2.3.2. Zeolite Supported Catalysts

Zeolites are microporous aluminosilicates with a general formula of [Al$_x$Si$_{1-x}$O$_2$$^{y-}$]$_x$ and consist of a negatively charged network that requires cationic counterions (e.g., Na$^+$, Ca^{2+}) for charge compensation. Through cation exchange and post-synthetic modification, zeolitic physicochemical properties, such as basicity and hydrophilicity, can be finely tuned. Furthermore, a transition metallic phase, such as Ni or Rh, can be introduced via ion-exchange or impregnation to prepare zeolite supported catalysts suitable for CO_2 methanation applications [88]. Graça et al. [96] were among the first to introduce Ni on ultrastable Y (USY) zeolites with Na$^+$ counter-ions for application as CO_2 methanation catalysts. Ni introduction via impregnation proved to be more suitable compared to introduction via ion-exchange because of the higher reducibility of impregnated NiO species, while a latter Ce addition improved the performance further via its synergy with the Ni metallic phase. Westermann et al. [97] studied the mechanism of CO_2 methanation over Ni/USY catalysts and concluded that CO_2 was initially weakly adsorbed over the Na$^+$ compensating cation sites on the zeolite. Following the initial chemisorption step, CO_2 hydrogenation proceeded via a CO intermediate adsorbed on the Ni particles.

Bacariza et al. [98] then performed an extensive work on the influence that several monovalent and divalent compensating cations exert over the CO_2 methanation performance of Ni/USY catalysts.

The compensating cations were ion-exchanged in the H-USY zeolite in its acidic form and the Ni phase was impregnated subsequently. Regarding the monovalent cations, a trend was observed where the CO_2 methanation performance (CO_2 conversion and CH_4 selectivity) increased for the heavier elements, following the order $Cs^+ > Na^+ > Li^+ > K^+ > H^+$ (with K^+ being an exception). These differences were attributed to the increase of the CO_2 adsorption capacity through a higher support alkalinity. Regarding the divalent cations, the catalytic activity followed a different trend by decreasing for the heavier elements in the order $Mg^{2+} > Ca^{2+} > Ba^{2+}$. The better performance for ion-exchange with Mg^{2+} was attributed to the higher Ni dispersion and Ni surface area. Thus, ion-exchange of compensating cations could be a correct pathway to tune specific properties of zeolite supported CO_2 methanation catalyst, such as metallic phase dispersion, support alkalinity and water affinity.

Besides the effect of different compensating cations, the optimization of the Si/Al ratio and the introduction of additional promoters (e.g., Mg, La and Ce) via impregnation has been studied. Bacariza et al. [99] modified the USY zeolitic composition in terms of Si/Al ratio and observed that higher Si/Al ratios decreased the water affinity and provided an enhanced methanation activity. Mg [68], La [100] and Ce [101] have also been employed as further promoters and introduced via impregnation over the zeolite support. The introduction of these promoters aimed to improve the dispersion of the metallic phase and promote CO_2 chemisorption via enhancing the surface basicity. Bacariza et al. [88] also presented some proposals for the preparation of active zeolite supported CO_2 methanation catalysts that incorporate properties such as high metallic phase dispersion, increased zeolite support basicity, low water affinity and sufficient steam resistance.

Lastly, Zhang et al. [102] prepared a novel methanation catalyst by using a Na-modified Y zeolite as a support and Al-source for the subsequent formation of a Ni-Al hydrotalcite precursor phase. After reduction, Ni-based, hydrotalcite-derived catalysts supported on the zeolitic structure were created. The catalysts exhibited a unique mosaic structure and the supported Ni nanoparticles were successfully confined by the AlO_x phase, thus improving their resistance to sintering and coke formation. Table 1 summarizes the CO_2 methanation performance of some typical catalysts promoted with group I and II metals.

2.4. Other Promoters that Favour CO_2 Chemisorption

Besides alkali and alkaline earth metals, lanthanides or rare earths, such as La, Ce and Pr [103], transition metals, such as V, W, Mn, Co and Fe [39,104,105], as well as noble metals, such as Pd, Pt, Rh and Ru [106], are commonly introduced into CO_2 methanation catalysts to enhance their activity. A common Ni-based catalyst promotion with metals, such as Ru, Rh, Pt, Co and Fe, mostly aims at the creation of bimetallic and alloy particles in order to improve the properties of the Ni metallic phase, such as reducibility, metal dispersion and resistance to oxidation, agglomeration and coking [8,28]. On the other hand, lanthanides and some transition metals often target the modification of the metal oxide support to improve properties such as surface basicity and oxygen vacancy concentration, leading to enhanced CO_2 chemisorption similarly to the promotion with alkali and alkaline earth metals [27,28].

Just like the works dealing with screenings performed using alkali and alkaline earth metals, Xu et al. [103] and Guilera et al. [107] screened several rare earth and transition metals (i.e., La, Ce, Sm, Pr, Y and Zr) as promoters over Ni/Al_2O_3 catalysts. Among them, Pr, Ce and La exhibited the most pronounced promoting effects. La-promotion specifically, has been reported to be beneficial for the CO_2 methanation performance by a number of studies, as it appears to enhance the support alkalinity. La-addition on the support can been performed either via separate impregnation [108,109] or via co-impregnation with Ni that targets the formation of an initial $LaNiO_3$ perovskite precursor phase [110,111]. Lastly, Mn promotion also targets similar improvements, namely enhancing the CO_2 adsorption and increasing the metal phase dispersion [104].

Table 1. Summary of some typical alkali and alkaline earth promoted catalysts on the methanation of CO_2.

Promoter	Catalyst	Synthesis Method	Conditions	Performance	Comments	Ref.
0.06–0.4% Li, Na, K and Cs	0.5% and 5% Ru/TiO$_2$	Wet impregnation	GHSV = 56,000 h^{-1} H$_2$/CO$_2$ = 4/1	X_{CO2} = 60%, S_{CH4} = 95% at 400 °C (0.2% Na on 0.5% Ru/TiO$_2$)	Catalytic activity improved after addition of small amounts of alkalimetals on 0.5% Ru/TiO$_2$. Less pronounced effect for 5% Ru/TiO$_2$	[33]
10% LiNO$_3$, NaNO$_3$, Na$_2$CO$_3$ and K$_2$CO$_3$	1% Ru/Al$_2$O$_3$	Incipient wetness impregnation	GHSV = 25,000 h^{-1} H$_2$/CO$_2$ = 4/1	X_{CO2} = 60%, S_{CH4} = 99% at 350 °C (10% LiNO$_3$ on 1% Ru/Al$_2$O$_3$)	Only LiNO$_3$ significantly promoted activity. Na$_2$CO$_3$ and K$_2$CO$_3$ masked Ru particles and suppressed methanation activity	[35]
5% Na, K, Mg and Ca	20% Co/Al$_2$O$_3$	Incipient wetness impregnation	H$_2$/CO$_2$ = 4/1	X_{CO2} = 52%, S_{CH4} = 67% at 400 °C (5% Na on 10% Co/Al$_2$O$_3$)	Na and K increased the population of basic sites but promoted CO selectivity. Mg and Ca did not favour methanation activity either, but prevented Co nanoparticle sintering	[37]
0.1–1% Na	33% Ni/SiO$_2$ and 13% Ni/CeO$_2$	Wet impregnation	H$_2$/CO$_2$ = 50/1	X_{CO2} = 85%, S_{CH4} = 85% at 250 °C (0.1% Na on 33% Ni/SiO$_2$)	Ni active surface area decreased upon Na addition. Negative impact on activity for Ni/CeO$_2$, but slightly positive impact for Ni/SiO$_2$	[41]
16.5% K and Ba	1% Rh/Al$_2$O$_3$	Flame spray pyrolysis	GHSV = 6000 h^{-1} H$_2$/CO$_2$ = 4/1	X_{CO2} = 25%, S_{CH4} = 0% at 375 °C (16.5 % K on 1% Rh/Al$_2$O$_3$)	K-addition led to pure CO production over the entire temperature range. Ba-modified catalyst slightly inferior to Rh/Al$_2$O$_3$ for CO$_2$ methanation	[43]
0.5–20% KOH	0.5–20% Ni/Al$_2$O$_3$	Incipient wetness impregnation	H$_2$/CO$_2$ = 4/1	X_{CO2} = 40%, S_{CH4} = 45% at 400 °C (10% K on 12% Ni/Al$_2$O$_3$)	Strongly adsorbed formate intermediates over KOH-modified catalysts favoured CO selectivity	[45]
1.7–7.6% K (x = 0.1–0.4 for La$_{1-x}$K$_x$NiO$_3$)	24–28.5% Ni/La$_2$O$_3$	Citrate sol-gel La$_{1-x}$K$_x$NiO$_3$ synthesis and reduction	GHSV = 48,000 h^{-1} H$_2$/CO$_2$ = 12.5/1	X_{CO2} = 50%, S_{CH4} = 45% at 306 °C (for x= 0.3 => La$_{0.7}$K$_{0.3}$NiO$_3$)	Easy-to-desorb CO species formed after K-doping stirred the reaction towards RWGS and CO selectivity	[51]

Table 1. *Cont.*

Promoter	Catalyst	Synthesis Method	Conditions	Performance	Comments	Ref.
4% MgO, CaO, SrO and BaO	10% Ni/SiO$_2$	Wet impregnation	GHSV = 15,000 h^{-1} H$_2$/CO$_2$ = 4/1	X$_{CO2}$ = 71%, S$_{CH4}$ = 99% at 300 °C (4% SrO on 10% Ni/SiO$_2$)	MgO inhibited activity, CaO had little effect, SrO and BaO enhanced activity, while SrO also promoted the catalyst stability	[52]
1–7.5% Mg, Ca, Sr and Ba	20% Ni/Al$_2$O$_3$	Incipient wetness impregnation	GHSV = 16,000 h^{-1} H$_2$/CO$_2$ = 4/1	X$_{CO2}$ = 80%, S$_{CH4}$ = 100% at 300 °C (5% Ba on 20% Ni/Al$_2$O$_3$)	Lighter elements Mg and Ca promoted CO selectivity, while heavier elements Sr and Ba favoured methanation	[53]
1.4% Mg, 2.2% Ca, 4.7% Sr and 7.2% Ba (Ce$_{0.9}$M$_{0.1}$O$_x$ support)	10% Ni/Ce$_{0.9}$M$_{0.1}$O$_x$	Citrate sol-gel modified CeO$_2$ synthesis and Ni incipient wetness impregnation	WHSV = 36,000 mL h^{-1} g^{-1} H$_2$/CO$_2$ = 4/1	X$_{CO2}$ = 70%, S$_{CH4}$ = 95% at 270 °C (10% Ni/Ce$_{0.9}$Ca$_{0.1}$O$_x$)	Ca-doping led to the highest methanation activity (with Sr being second-to-best). TOF$_{Ni}$ could be linearly correlated to the amount of oxygen vacancies and moderately strong basic sites on the support surface	[30]
1–4% MgO	10% Ni/SiO$_2$	Sequential wet impregnations and co-impregnation	WHSV = 36,000 mL h^{-1} g^{-1} H$_2$/CO$_2$ = 4/1	X$_{CO2}$ = 65%, S$_{CH4}$ = 98% at 400 °C (1% Mg on 10% Ni/SiO$_2$)	1% MgO introduced by co-impregantion led to the highest catalytic activity and stability. Higher MgO contents blocked some Ni active sites	[63]
0.4–2.5% Mg (Change in Ni/Mg molar ratio)	6% Ni/ZrO$_2$	Citrate complexing method	WHSV = 15,000 mL h^{-1} g^{-1}, p = 0,1 MPa, H$_2$/CO$_2$ = 4/1	X$_{CO2}$ = 90%, S$_{CH4}$ = 100% at 250 °C (1% Mg on 6% Ni/ZrO$_2$)	Mg-addition led to Ni nanoparticle confinement, as well as resistance to sintering and coke formation	[64]
0.5–5% Mg	12% Ni/Al$_2$O$_3$ (OMA)	Evaporation-induced self-assembly (EISA)	GHSV = 15,000 h^{-1} H$_2$/CO$_2$ = 4/1	X$_{CO2}$ = 65%, S$_{CH4}$ = 96% at 300 °C (2.5% Mg on 12% Ni/Al$_2$O$_3$)	Mg-dopant increased the surface basicity of the catalysts and facilitated the chemisorption and activation of CO$_2$	[65]

Table 1. *Cont.*

Promoter	Catalyst	Synthesis Method	Conditions	Performance	Comments	Ref.
1% Mg	α-Fe$_2$O$_3$	Incipient wetness impregnation	GHSV = 150,000 h^{-1}, p = 8 bar, H$_2$/CO$_2$ = 4/1	X_{CO2} = 22%, S_{CH4} = 9% at 400 °C after 18 h (2.% Mg on α-Fe$_2$O$_3$)	Improved CO$_2$ adsorption over the Mg-modified Fe catalyst led to highly active Fe carbides and better methanation performance	[72]
0.8–8% Ca	12% Ni/Al$_2$O$_3$ (OMA)	Evaporation-induced self-assembly (EISA)	GHSV = 15,000 h^{-1} H$_2$/CO$_2$ = 4/1	X_{CO2} = 70%, S_{CH4} = 98% at 300 °C (6.4% Ca on 12% Ni/Al$_2$O$_3$)	Increased surface alkalinity of the support led to enhanced CO$_2$ chemisorption and lower activation energy for CO$_2$ methanation	[74]
2% CaO	1% Ru, 10% Ni/Al$_2$O$_3$ (OMA)	Evaporation-induced self-assembly (EISA)	WHSV = 30,000 mL h^{-1} g^{-1} H$_2$/CO$_2$ = 4/1	X_{CO2} = 80%, S_{CH4} = 98% at 360 °C (2% CaO on 0.8% Ru, 8% Ni/Al$_2$O$_3$)	Step increase in the CO$_2$ conversion and CH$_4$ selectivity after adding Ru second metal and CaO promoter	[75]
0.7% Ca	5% Ni/Ca$_x$Zr$_{1-x}$O$_{2-\delta}$	Wet impregnation	H$_2$/CO$_2$ = 4/1	X_{CO2} = 72%, S_{CH4} = 100% at 350 °C (0.7% Ca on 5% Ni/Ca$_x$Zr$_{1-x}$O$_{2-\delta}$)	Oxygen vacancies-coordinately unsaturated sites (cus) pairs facilitated the C-O bond scission, a crucial step during CO$_2$ methanation	[82]
0.1–1% Ca (x = 0.01–0.1 for Ca$_x$Ni$_{1-x}$TiO$_{3-\delta}$)	30% Ca-NiTiO$_3$/Al$_2$O$_3$ (11.5% Ni)	Coprecipitation Ca-NiTiO$_3$ synthesis and wet impregnation	GHSV = 5000 h^{-1} H$_2$/CO$_2$ = 4/1	X_{CO2} = 55%, S_{CH4} = 99.7% at 350 °C (0.5% Ca on 30% Ca-NiTiO$_3$/Al$_2$O$_3$)	Ca-doping on NiTiO$_3$ A-site promoted the formation of oxygen vacancies in close proximity to active Ni and therefore the chemisorption of CO$_2$	[84]
14% Mg	59% Ni/MgO-Al$_2$O$_3$	Coprecipitation hydrotalcite synthesis and reduction	WHSV = 1100 min^{-1} g^{-1} H$_2$/CO$_2$ = 4/1	X_{CO2} = 70%, S_{CH4} = 90% at 315 °C(14% Mg on 59% Ni/MgO-Al$_2$O$_3$)	Stable performance, as well as sintering and coking resistance for the hydrotalcite-derived catalysts	[89]

Table 1. *Cont.*

Promoter	Catalyst	Synthesis Method	Conditions	Performance	Comments	Ref.
6.1–28.5% Mg	17.2–57.8% Ni/MgO-Al$_2$O$_3$	Coprecipitation hydrotalcite synthesis and reduction	GHSV = 2400 h^{-1} H$_2$/CO$_2$ = 4/1	X_{CO2} = 97.9%, S_{CH4} = 97.5% at 250 °C (17.3% Mg on 37.5% Ni/MgO-Al$_2$O$_3$	Far superior low-temperature CO$_2$ conversion for Mg-containing hydrotalcite-derived catalysts, due to the increased surface alkalinity	[90]
0.3–12% Li, Na, K, Cs, Mg, Ca and Ba	15% Ni/USY zeolite	Ion-exchange for cations and Ni incipient wetness impregnation	GHSV = 43,000 h^{-1} H$_2$/CO$_2$ = 4/1	X_{CO2} = 62%, S_{CH4} = 92% at 375 °C (12.1% Cs in 15% Ni/Cs-exchanged USY)	Greater size for monovalent cations improved CO$_2$ adsorption (Cs$^+$ > Na$^+$ > Li$^+$ > H$^+$), while Mg^{2+} benefited Ni dispersion	[98]
0.9–13% Mg	4.8–15% Ni/USY zeolite	Ion-exchange or impregnation for Mg and Ni incipient wetness impregnation	GHSV = 43,000 h^{-1} H$_2$/CO$_2$ = 4/1	X_{CO2} = 65%, S_{CH4} = 93% at 400 °C (0.7% Mg in 15% Ni/Mg-exchanged USY)	Finer and better-dispersed Ni nanoparticles after Mg impregnation or Mg ion-exchange	[68]

3. Alkali and Alkaline Earth Metals as Active Sorbents Phases in the Combined Capture and Methanation of CO_2

Carbon capture and utilization (CCU) revolves around the concept of coupling post-combustion CO_2 capture to a CO_2 utilization step [5]. If this step is an exothermic reduction reaction, then the energy released can be used to mitigate the energy demands arising from the endothermic CO_2 desorption step. Additionaly, CH_4 selectivity for many catalysts during CO_2 hydrogenation is high at temperatures that can coincide with those required for CO_2 desorption, thus rendering CH_4 as a preferable final product. The combination of these two processes, namely CO_2 adsorption and hydrogenation, in a single reactor can be realized via the development of novel dual-function materials (DFMs) that embody both adsorption and catalytic capabilities [19,20,25].

In most DFM materials targeting CH_4 production, Ru is chosen as the preferred metal to provide the catalytically active sites, despite it being significantly less abundant and pricier compared to Ni. Since most flue gases are O_2-rich, a partial oxidation of the metallic surface takes place during the CO_2 capture step under practical operation conditions. The catalyst then needs to be reactivated under a H_2-rich gas flow. Ru is most promising in this regard, since the oxidized RuO_x layers can be re-reduced under H_2 flow at temperatures where CO_2 capture takes place (< 350 °C), thereby increasing the process energy efficiency by operating both steps isothermally [22]. Oxidized NiO requires more intense reducing environments to be reactivated, depending also on the support used and the type and loading of the adsorbent phase. A higher temperature activation step or the absence of O_2 from the CO_2-containing gas are thus necessary prerequisites for the employment of Ni-based DFMs [21,112]. By promoting a Ni catalyst with a second metal though, its reducibility could be enhanced in order for it to meet the requirements to be used under more practical flue-gas applications [23].

3.1. Ru-Based Dual-Function Materials

Duyar et al. [19] introduced the concept of a DFM for the CO_2 capture and conversion to CH_4 (Figure 8) [113]. The materials were prepared via incipient wetness impregnation, either impregnating $Ca(NO_3)_2$ first and then $Ru(NO)(NO_3)_2$ on γ-Al_2O_3, or vice versa. The loadings of the adsorbent (CaO) and the catalyst (Ru) were varied between 1 and 10 wt.%. It was shown that first impregnating the sorbent and then the catalyst was a more suitable route for the material preparation, whereas a high sorbent loading appeared to be beneficial, since it increased the amount of captured CO_2 and the extent of CO_2 spillover towards the methanation active sites. An optimum composition of 5% Ru, 10% CaO/γ-Al_2O_3 produced the maximum amount of CH_4 per kg of DFM material at 0.5 mol CH_4/kg DFM (or 0.5 mmol CH_4/g DFM). The authors also showed that the high dispersion of the CaO sorbent phase, that can facilitate a reversible chemisorption and desorption of CO_2 at moderate temperatures, in combination with the easily reducible and highly active Ru methanation catalyst, could enable the whole process to proceed isothermally at 320 °C. A follow up parametric study [114] reported an effective DFM preparation method, as well as suitable adsorption and methanation conditions in order for it to be applied to industrial-scale applications.

Following the earlier works, Duyar et al. [113] also used Rh as the active metal with CaO adsorbent phase and they showed that a comparatively miniscule amount of Rh loading in the DFM (0.1 wt.%) could generate comparable amounts of CH_4 with a 5% Ru loading. However, the high price of Rh is still a major problem and thus, the less expensive Ru is considered as a more suitable active metal. In the second part of their work, Duyar et al. [113] tested K_2CO_3, Na_2CO_3 and MgO as potential CO_2 sorbent alternatives. K_2CO_3 and Na_2CO_3 exhibited better results, with the 5% Ru, 10% Na_2CO_3/γ-Al_2O_3 DFM yielding 1.05 mol CH_4 per kg material at 320 °C operation. Thus, it was shown that the optimization of the CO_2 sorption phase can be of equal importance to that of the catalytically active metal phase in an attempt to lower the catalyst material costs and increase the process efficiency. A parametric study was also conducted for the new optimized 5% Ru, 10% Na_2CO_3/γ-Al_2O_3 DFM [115]. Two parallel reactors, one operating under CO_2 capture and the other under CO_2 methanation conditions, could lead to an

optimal use of available resources, while prolonged operation did not appear to be detrimental for the material and its catalytic properties.
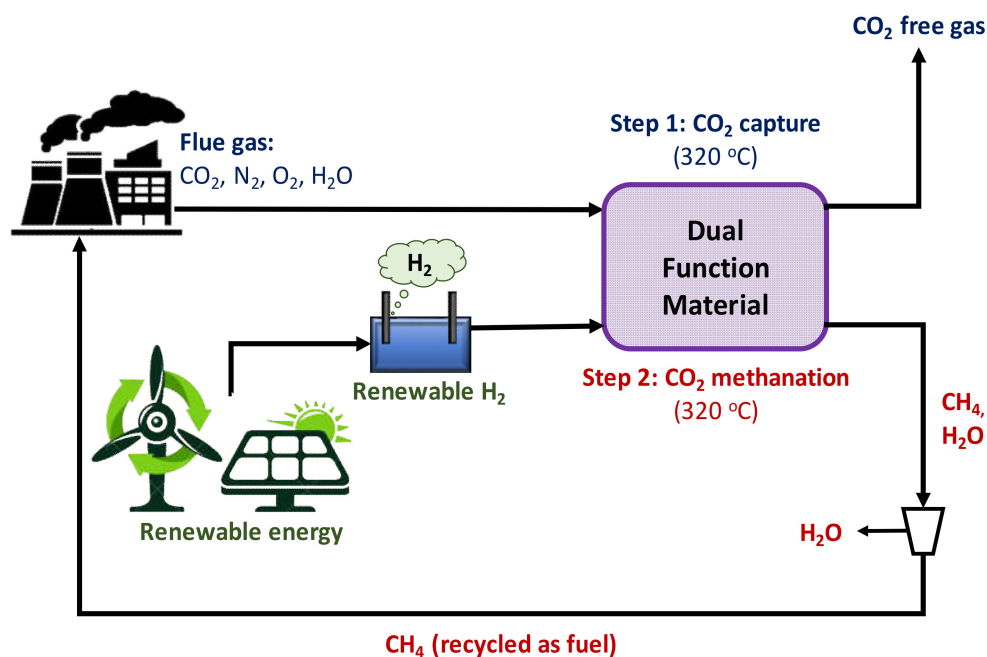

Figure 8. Schematic summarizing the dual-function materials (DFM) concept (adopted from [113]).

Due to its easy reduction once oxidized, ruthenium's role is crucial for isothermal DFM applications and it can provide stable performance [22]. From a kinetic point of view, Ru-based DFMs (5% Ru) appearred to achieve faster hydrogenation rates, even compared to their Rh-based analogues (0.5% Rh), when Na_2CO_3 (or "Na_2O") was used as sorbent. Thus, Ru can be considered a superior DFM catalyst phase based on price and reaction kinetics criteria. Regarding the sorbent's impact on the methanation kinetics, "Na_2O"-type active sorbents appeared far superior and led to an overall higher CH_4 yield, despite CaO sorbents initially providing a higher CO_2 adsorption capacity [21].

The mechanism behind the two-step CO_2 capture and methanation process over the 5% Ru, 10% Na_2CO_3/γ-Al_2O_3 (or 5% Ru, 6.1% "Na_2O"/γ-Al_2O_3) DFM was highlighted by Proaño et al. [116] employing in-situ DRIFTS (Figure 9). After calcination and pre-reduction of the materials, Na_2CO_3 was decomposed and Na-rich surface, as well as Al-O$^-$-Na$^+$ sites, were created and denoted as "Na_2O". On Na-free Ru/Al_2O_3, CO_2 was chemisorbed at Ru sites and at –OH groups of the support, whereas on the Na-containing DFM, CO_2 was chemisorbed at Al-O-Na$^+$ sites in large quantities. The presence of Na$^+$ on the surface caused CO_2 to be primarily adsorbed in the form of chelated carbonato complexes, while the Ru and Al-OH sites could still accommodate adsorbed CO_2, as in Ru/Al_2O_3. The adsorbed bidentate carbonates could then spillover to adjacent Ru catalytically active sites, where they were hydrogenated into CH_4 via formate-type intermediates. Enhanced CH_4 production for the Na-containing DFM was thus attributed to the larger CO_2 capture capacity, due to the additional Al-O-Na$^+$ sites that had a high affinity towards CO_2.

Besides the Farrauto group, Bermejo-López et al. [24] performed a thorough work to describe the mechanism of CO_2 capture and methanation, as well as to correlate the type and loading of the adsorbent phase with the material's performance (Figure 10). Ru metal dispersion was one parameter dependant on the adsorbent type, with CaO seeming to hinder it, while Na_2CO_3 promoting it. The basicity of the materials increased with higher adsorbent loading and this promoted the CH_4 yield. CaO provided strong basic sites, where CO_2 was chemisorbed forming stable carbonates ($CaCO_3$) that required higher temperatures to be desorbed. On the other hand, medium-strength basic sites

over Na_2CO_3 led to the formation of less stable carbonates, enabling operation at lower temperatures. The proposed reaction mechanism involved an initial adsorption of CO_2 with simultaneous release of H_2O from the sorption active phases. During the following methanation step, adsorbed CO_2 spilled over to Ru sites and was hydrogenated to methane, while a delay in the H_2O signal could be attributed to some H_2O-product being adsorbed by the basic sorbent sites and forming $Ca(OH)_2$ and $NaOH$.
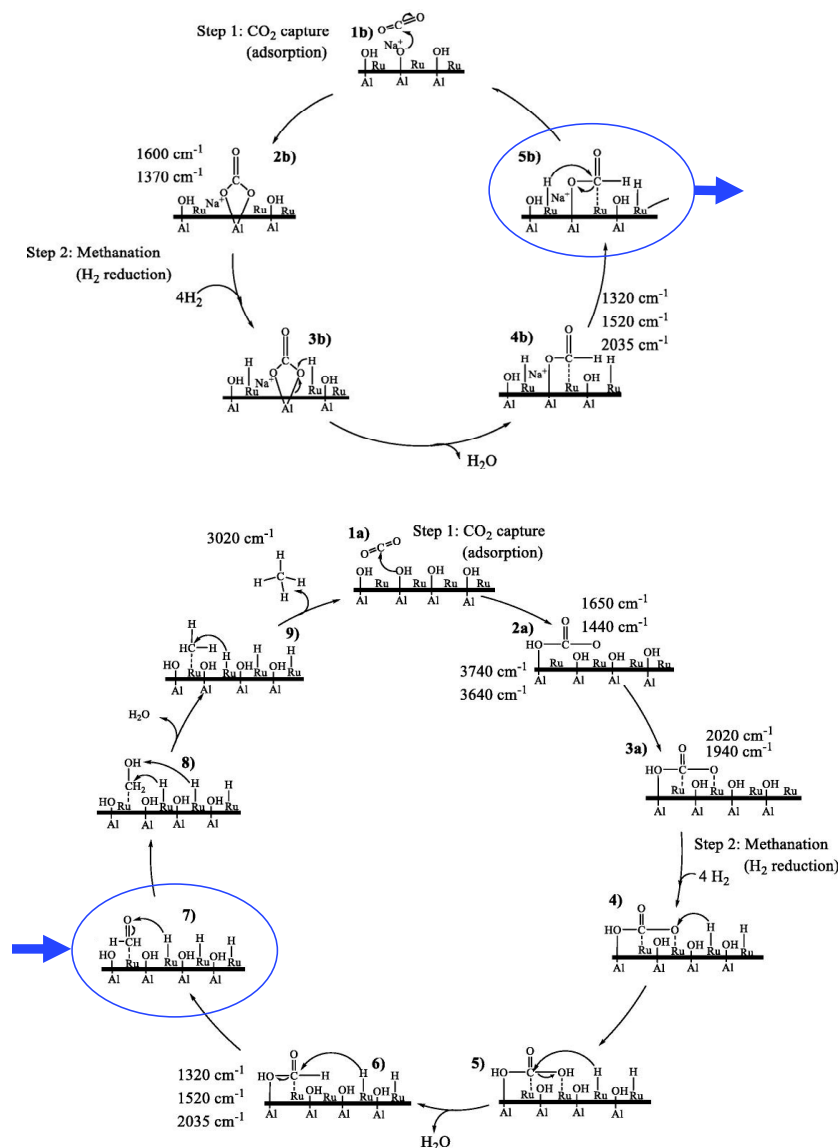
Figure 9. Proposed CO_2 methanation mechanism over 5%Ru/Al_2O_3 (down) and extended (up and down) for over 5%Ru, 6.1%"Na_2O"/Al_2O_3 DFM. Reproduced with permission from ref. [116]. Copyright 2019 Elsevier.

Cimino et al. [35] modified the γ-Al_2O_3 support with various alkali metals (Li, Na, K and Cs) and 1% Ru was chosen as the active metal phase. Regarding CO_2 methanation performance, only Li exhibited a promotion effect and formed Li-aluminate spinel-phases that stabilized the alumina support and its interaction with Ru active sites. During cyclic CO_2 capture and methanation at low temperature (230 °C), the Li-promoted material presented faster methanation kinetics and higher CH_4 production compared to the Na-promoted one. It was noted that the temperature of the cyclic operation for the Li-promoted 1% Ru DFM (230 °C) was considerably lower compared with that for other DFMs that have higher Ru loadings.
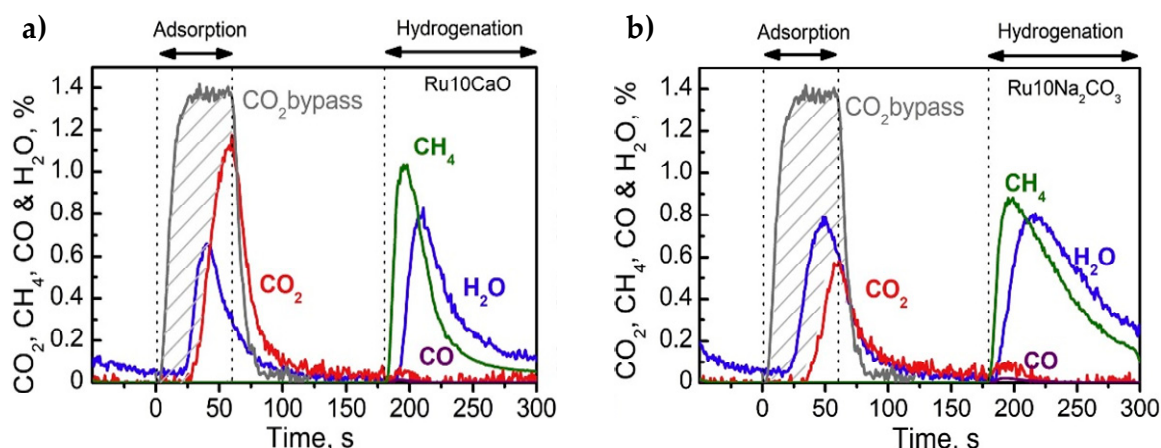
Figure 10. CO_2, H_2O, CH_4 and CO concentration profiles during one CO_2 adsorption and hydrogenation cycle at 370 °C with (**a**) Ru10CaO and (**b**) Ru10Na$_2$CO$_3$ samples. Reproduced with permission from ref. [24]. Copyright 2019 Elsevier.

Lastly, Sun et al. [25] employed a DFM consisting of a Ru supported on CeO_2 nanorods methanation catalyst and an alkali nitrate promoted MgO sorbent mechanically mixed together (Figure 11). It has been already reported by Wang et al. [117] that the CO_2 methanation mechanism over Ru/CeO_2 follows a different pathway compared to Ru/Al_2O_3, with the oxygen vacancy catalyzed formate dissociation being the rate determining step in the former. Sun et al. [25] performed the integrated CO_2 capture and methanation process in their DFM at 300 °C. CO_2 was initially captured in the form of $MgCO_3$. Subsequently, during the methanation process, CO_2 was desorbed and activated by an oxygen vacancy in the CeO_2 nanorod support, forming a formate intermediate. The formate was then decomposed into a ruthenium carbonyl and further hydrogenated into CH_4 by nearby hydrogen atoms chemisorbed at the Ru surface. It was further noted that, although CH_4 yield and CO_2 conversion were higher for 10% Ru loading during the 1st cycle, the 5% Ru loaded catalyst showed better performance during the 10th cycle, probably due to the better preservation of the oxygen vacancies in the support.
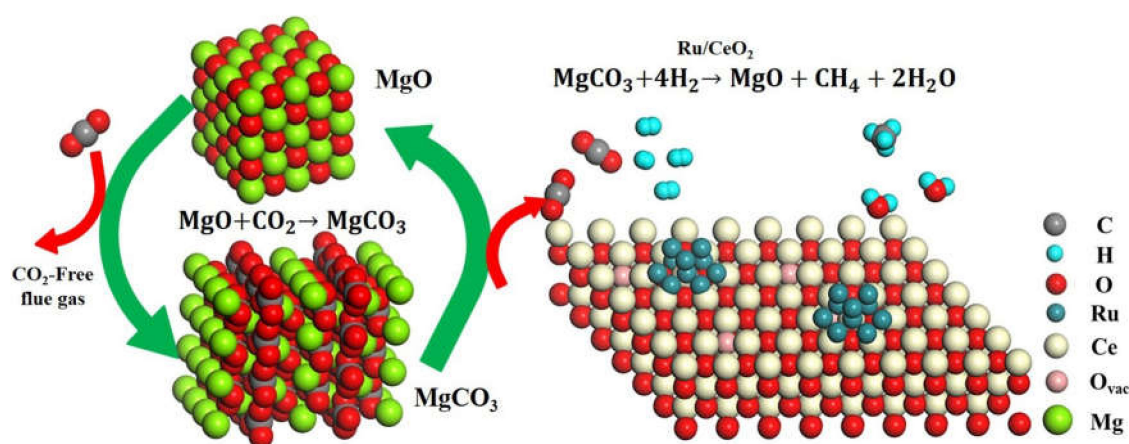

Figure 11. Schematic illustration for the CO_2 capture from the MgO sorbent phase and the conversion of captured CO_2 into CH_4 over the Ru/CeO_2 catalyst phase. Reproduced with permission from ref. [25]. Copyright 2020 Elsevier.

3.2. Ni-Based Dual-Function Materials

Although Ni would be a more suitable choice as a methanation catalyst in DFMs, being considerably cheaper and more abundant compared to noble metals like Ru and Rh, there are a number of limitations that need to be carefully considered. Arellano-Treviño et al. [21] impregnated Ni on a γ-Al_2O_3 carrier

that had been previously loaded with a Na_2CO_3 adsorbent and the Ni-based DFM underwent a pre-reduction at 650 °C for the catalyst activation. The authors showed that the Ni-based DFM (10% Ni, 6.1% "Na_2O"/γ-Al_2O_3) operated cyclically at a constant 320 °C temperature could only produce substantial amounts of CH_4, if the CO_2 capture step was performed under an O_2-free gas (7.5% CO_2/N_2). On the other hand, if the CO_2 capture step was performed at 320 °C under a simulated flue-gas (7.5% CO_2, 4.5% O_2, 15% H_2O, balance N_2), no CH_4 was produced during the subsequent hydrogenation step at the same temperature. This was explained by the inability of NiO to be reactivated under 15% H_2/N_2 at 320 °C in order for the whole operation to proceed isothermally. Furthermore, Ni-based DFMs retained a certain amount of preadsorbed CO_2 that was not further converted.

Following their earlier work, Arellano-Treviño et al. [23] attempted to enhance the Ni-based material's reducibility by introducing small amounts (0.1 and 1 wt.%) of noble metals Ru, Pt and Pd. Pd-containing samples exhibited comparatively inferior performance, whereas the beneficial effect of Pt and Ru addition rested on the enhancement of NiO reducibility under 13.26% H_2/N_2 flow at 320 °C. 1 wt.% Pt addition caused 50% of the initially oxidized NiO to be reduced, while this value for the promotion with 1 wt.% Ru reached 70%. The authors speculated that PtO_x and RuO_x species reduced rapidly and the exposed Pt and Ru active surfaces splitted H_2 molecules and helped reduce the adjacent NiO sites. For cyclic operation at 320 °C, the 1% Ru, 10% Ni, 6.1% "Na_2O"/γ-Al_2O_3 material exhibited great cyclic stability and the highest CH_4 production, since both Ru and Ni sites are active for CO_2 methanation. Compared to the Ni-free DFM with the same Ru loading (1% Ru, 6.1% "Na_2O"/γ-Al_2O_3), the Ni-containing one (1% Ru, 10% Ni, 6.1% "Na_2O"/γ-Al_2O_3) exhibited an increased CO_2 adsorption capacity and CH_4 yield, at a cost, however, of slower methanation kinetics. As such, the synergy between Ni and Ru metals promoted the material's performance, in agreement with other studies regarding CO_2 methanation [75,118].

Other works typically perform the CO_2 capture step with an O_2-free gas mixture of CO_2 balanced with a carrier gas. Bermejo-López et al. [112] studied the effects of Ni, as well as CaO and Na_2CO_3 loadings on the DFM performance (Figure 12). The addition of the adsorbent phase weakened the metal-support interaction and enhanced the reducibility of the Ni metallic phase. Similarly to their previous work [24], the authors showed that CaO adsorbent led to the creation of highly stable carbonates that required higher temperatures to decompose, while less stable carbonates over Na_2CO_3 decomposed at a lower temperature. Thus, during the following hydrogenation step, CH_4 formation was favoured at higher temperatures when CaO was used as the active sorbent, peaking at 520 °C, while maximum CH_4 was produced for Na_2CO_3 at 400 °C. Increasing the Ni loading resulted in increased CO_2 sorption capacity and CH_4 production. Regarding the proposed mechanism, CO_2 was initially adsorbed over NaOH and $Ca(OH)_2$ species, with H_2O being simultaneously released. During the subsequent H_2/N_2 inflow, adsorbed CO_2 was reduced after its spillover to Ni sites and detected product H_2O was delayed due to its initial adsorption by the sorbent phases. The DFM with CaO sorbent (10NiCa) exhibited a higher CH_4 selectivity upon hydrogenation during cyclic operation at 400 °C, while the DFM with Na_2CO_3 sorbent (10NiNa) produced more CO arising from the RWGS reaction.

Chai et al. [119] also tested the effects of different CO_2 adsorbents (MgO, CaO, Na_2CO_3 and K_2CO_3) on Ni-based DFMs supported on Al_2O_3. The catalyst and adsorbent loadings were the same, at 10 wt.%, while the CO_2 capture step was performed under an O_2-free 9.5% CO_2/N_2 gas flow. In a similar fashion to the findings of Bermejo-López et al. [23,102], the authors showed that CaO sorbent led to greater CO_2 sorption capacity. However, the release of adsorbed CO_2 in the material with CaO sorbent was not fully reversible. The material with Na_2CO_3 sorbent exhibited a high CO_2 capture capacity, along with a high release efficiency. Hence, methanation capacity for the material with Na_2CO_3 sorbent was superior, a property attributed to the easier release and spillover of adsorbed CO_2 towards the Ni catalytically active sites.
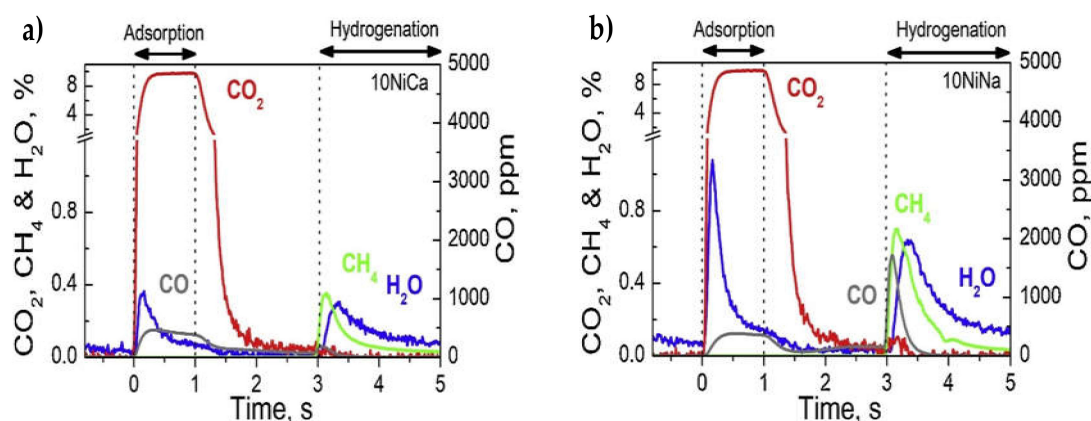
Figure 12. CO_2, H_2O, CH_4 and CO concentration profiles during one CO_2 adsorption and hydrogenation cycle at 400 °C with (**a**) 10NiCa and (**b**) 10NiNa catalysts. Reproduced with permission from ref. [112]. Copyright 2019 Elsevier.

Hu et al. [120] prepared Ni-based DFMs supported on ZrO_2 and modified with La and K. The use of K and La promoters raised the CO_2 sorption capacity of the materials, with the K-modified material increasing its CO_2 capture efficiency four-fold, compared with the unmodified one. K-promoted Ni/ZrO_2 released CH_4 upon hydrogenation much slower, while the La-promoted material exhibited faster methanation kinetics, with the time required for CH_4 release roughly matching the time required for CO_2 capture. The methanation mechanism was modified upon K-promotion and additional less-reducible intermediate bidentate carbonates were formed, whereas the reaction over unpromoted and La-modified Ni/ZrO_2 proceeded over active formate intermediates. It could be concluded, that La-promotion was more suited for operation at lower temperatures (250 °C) by achieving favourable kinetics, while K-modification favoured increased CO_2 chemisorption and methanation efficiency at higher temperatures (>350 °C).

Finally, Zhou et al. [121] prepared a 2D-layered Ni/MgO-Al_2O_3 material to be used during the integrated CO_2 capture and methanation (Figure 13). The layered oxides resulted after calcination and reduction of the initial hydrotalcite (or layered double hydroxide) precursors, which were in turn prepared via the coprecipitation method. By increasing the Ni content in the material, the interaction between Ni and the MgO-Al_2O_3 support weakened and Ni species became more reducible. For the cyclic CO_2 capture and methanation process, the authors aimed at optimizing the respective durations, so that CO_2 breakthrough was minimal and a maximum utilization of reactant H_2 was achieved. Complete capture and methanation could be achieved by a 35 s CO_2 sorption time and a 25 s methanation time. Upon conducting in-situ FTIR experiments, monodentate and bidentate carbonates, as well as formate species were detected during the CO_2 sorption phase. Following 20% H_2/Ar flow, the observed bands suggested a gradual removal of these species via hydrogenation to CH_4, with no CO being detected. Further development of materials derived from hydrotalcite precursors containing Mg and Ni could be favourable for DFM applications, since Ni can be highly dispersed and stabilized, while a high Mg content can provide a plethora of surface basic sites for CO_2 chemisorption [90]. Table 2 summarizes the performance of DFMs for the combined capture and methanation of CO_2.
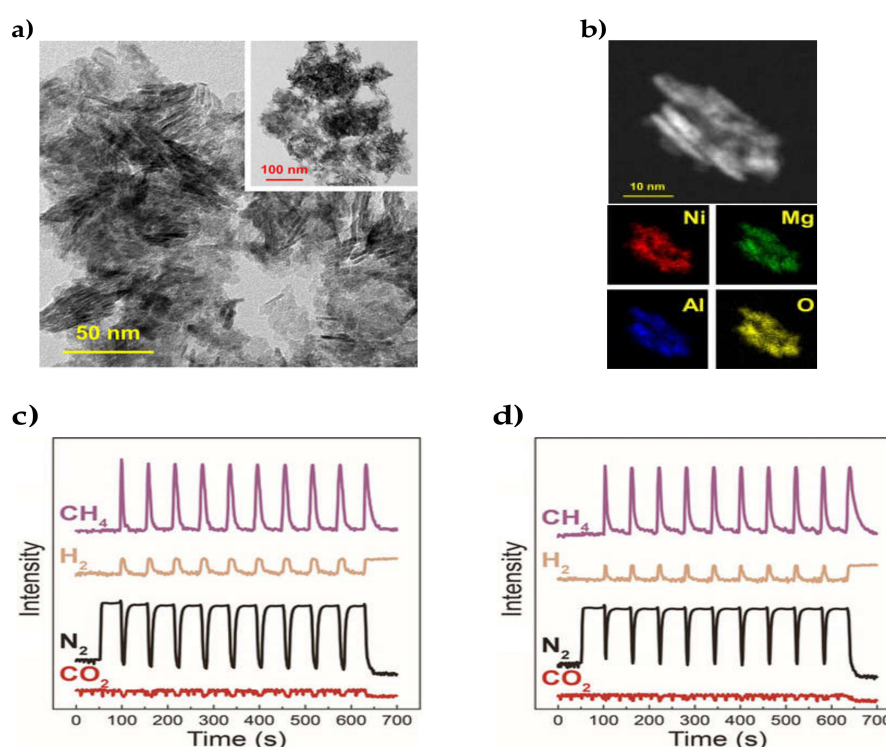
Figure 13. (**a**) TEM images and (**b**) EDX Mapping of 2.0NiMgAl-LDO. Continuous CO_2 capture and methanation over 2.0NiMgAl-LDO-re at 250 °C (Adsorption: 15 vol % CO_2/N_2 (70 mL min^{-1}), 1 bar; methanation: 100 % H_2 (70 mL min^{-1}), 1 bar); (**c**) $t_{adsorption}$ = 30 s, $t_{methanation}$ = 30 s; and (**d**) $t_{adsorption}$ = 35 s, $t_{methanation}$ = 25 s. Reproduced with permission from ref. [121]. Copyright 2019 Wiley.

3.3. Dual-Function Materials for Products Other than Methane

Apart from synthetic natural gas (SNG) obtained during methanation, the concept of DFMs for the integrated CO_2 capture and conversion has been extended for the production of CO and syngas, that can be used for the further production of other value-added products. Bobadilla et al. [122] prepared a K-promoted trimetallic FeCrCu catalyst supported on $MgO-Al_2O_3$. The K-component was added to increase the CO_2 sorption capacity, while the combination of three earth-abundant metals (Fe, Cr and Cu) favoured CO selectivity via RWGS. Hyakutake et al. [123] promoted a Cu/Al_2O_3 catalyst with K and Ba for CO_2 capture and conversion to CO. K-promotion facilitated Cu dispersion and resulted in a very high capacity for CO_2 capture as formate intermediates. These intermediates were then selectively reduced to CO via the RWGS route. The Ba-promoted material captured much less CO_2 in comparison and thus exhibited an inferior performance as DFM for CO production.

Al-Mamoori et al. [124] introduced a new feature via the use of K and Na-promoted CaO and MgO-based double salts as the CO_2 adsorbing components, in an attempt to greatly increase the CO_2 capture efficiency and sorption kinetics. The K-Ca, Na-Ca, K-Mg and Na-Mg double salts were supported on γ-Al_2O_3 via the impregnation of alkalimetal carbonates and alkaline earth metal nitrates, whereas Ni was impregnated subsequently. After the CO_2 capture step, ethane was flowed into the reactor in order to produce syngas via the dry reforming of ethane (DER) reaction.

Additionally, Sun et al. [125] employed a common CO_2 sorbent, CaO, directly as support material for Ni nanocatalysts with adjacent Ce-species. They argued that the already established calcium-looping process that rests on the carbonization and calcination of CaO for CO_2 capture and sequestration (CCS) could be modified through the integration of a CO_2 utilization step by converting CO_2 to CO. The incorporation of Ni facilitated CO_2 reduction, whereas Ce-species provided oxygen vacancies that were active sites for CO_2 dissociation and prevented the agglomeration of individual CaO and Ni nanocrystallites.

Table 2. Summary of dual-function materials (DFMs) employed in the combined CO_2 capture and methanation process.

CO_2 Sorbent	Catalyst	CO_2 Capture Conditions	CO_2 Methanation Conditions	CH_4 Production [mmol CH_4/g DFM]	Comments	Reference
1–10% CaO	1–10% Ru/Al$_2$O$_3$	10% CO_2/N$_2$, 320 °C, 30 min	4% H$_2$/N$_2$, 320 °C, 2 h	**0.50** (5% Ru, 10% CaO/Al$_2$O$_3$)	High sorbent loading increased CO_2 spillover to Ru active sites. 5% Ru, 10%CaO/Al$_2$O$_3$ as best composition. Cyclic operation at 320 °C	[19]
10% CaO, MgO, Na$_2$CO$_3$ and K$_2$CO$_3$	0.1–10% Rh and 5% Ru/Al$_2$O$_3$	10% CO_2/N$_2$, 320 °C, 30 min	4% H$_2$/N$_2$, 320 °C, 2 h	**0.4** (0.1% Rh, 10% CaO/Al$_2$O$_3$), **1.05** (5% Ru, 10% Na$_2$CO$_3$/Al$_2$O$_3$)	0.1% Rh was quite active but Rh is pricy. Na$_2$CO$_3$ constituted a better adsorbent than CaO for Ru-based DFMs	[113]
10% CaO, MgO, Na$_2$CO$_3$ (6.1% "Na$_2$O") and K$_2$CO$_3$ (7.01% "K$_2$O")	0.5% Rh and 5% Ru/Al$_2$O$_3$	10% CO_2/N$_2$, 320 °C, 30 min	10% H$_2$/N$_2$, 320 °C, 1 h	**0.614** (5% Ru, 6.1% "Na$_2$O"/Al$_2$O$_3$)	Ru-based DFMs with Na$_2$CO$_3$ achieved the fastest hydrogenation rates	[21]
5–15% CaO and Na$_2$CO$_3$	4% Ru/Al$_2$O$_3$	11% CO_2/Ar, 280–400 °C, 1 min	10% H$_2$/Ar, 280–400 °C, 2 min	**0.414** at 400 °C (4% Ru, 15% CaO/Al$_2$O$_3$), **0.383** at 310 °C (4% Ru, 10% Na$_2$CO$_3$/Al$_2$O$_3$)	Higher sorbent loading promoted CH_4 yield. More stable carbonates formed on CaO required higher temperature to decompose	[24]
10% LiNO$_3$, NaNO$_3$, Na$_2$CO$_3$ and K$_2$CO$_3$	1% Ru/Al$_2$O$_3$	15% CO_2/Ar, 230 °C, 30 min	12% H$_2$/Ar, 230 °C, 30 min	Not reported	Li-promoted DFM presented faster methanation kinetics. Operation at just 230 °C, a lower temperature compared with other DFMs	[35]
200% High-capacity MgO sorbent	2.5–10% Ru/CeO$_2$	65% CO_2/N$_2$, 300 °C, 1 h	5% H$_2$/N$_2$, 300 °C,	**6.60**, 1. cycle **3.36**, 10. cycle (5% Ru/CeO$_2$ + 200% MgO)	High CO_2 capture capacity due to a large MgO content. Mechanism: oxygen vacancy catalyzed CO_2 hydrogenation through a formate intermediate	[25]
10% Na$_2$CO$_3$ (6.1% "Na$_2$O")	10% Ni/Al$_2$O$_3$	7.5% CO_2/N$_2$ and 7.5% CO_2, 4.5% O$_2$, 15% H$_2$O/N$_2$, 320 °C, 20 min	15% H$_2$/N$_2$, 320 °C, 1 h	**0.276**, Without O$_2$ during CO_2 capture **0**, With O$_2$ during CO_2 capture (10% Ni, 6.1% "Na$_2$O"/Al$_2$O$_3$)	Ni-based DFMs required a prereduction/activation step at 650 °C and an O$_2$-free gas during CO_2 capture in order to produce CH_4	[21]

Table 2. *Cont.*

CO$_2$ Sorbent	Catalyst	CO$_2$ Capture Conditions	CO$_2$ Methanation Conditions	CH$_4$ Production [mmol CH$_4$/g DFM]	Comments	Reference
10% Na$_2$CO$_3$ (6.1% "Na$_2$O")	0.1–1% Ru, Pt, Pd with 10% Ni/Al$_2$O$_3$	7.5% CO$_2$, 4.5% O$_2$, 15% H$_2$O/N$_2$, 320 °C, 20 min	15% H$_2$/N$_2$, 320 °C	**0.38** (1% Ru, 10% Ni, 6.1% "Na$_2$O"/Al$_2$O$_3$)	Pt and Ru addition as second metals promoted NiO reducibility. Ni and Ru synergy led to the highest CH$_4$ yield	[23]
5–15% CaO and Na$_2$CO$_3$	5–15% Ni/Al$_2$O$_3$	10% CO$_2$/Ar, 280–520 °C, 1 min	10% H$_2$/Ar, 280–520 °C, 2 min	**0.142** at 520 °C (15% Ni, 15% CaO/Al$_2$O$_3$), **0.185** at 400 °C (10% Ni, 10% Na$_2$CO$_3$/Al$_2$O$_3$)	The adsorbent phase enhanced NiO reducibility. Methanation was favoured at higher temperatures when CaO was used as sorbent	[112]
10% CaO, MgO, Na$_2$CO$_3$ and K$_2$CO$_3$	10% Ni/Al$_2$O$_3$	9.5% CO$_2$/N$_2$, 320 °C, 25 min	10% H$_2$/N$_2$, 320 °C, 20 min	**0.140** (10% Ni, 10% CaO/Al$_2$O$_3$) **0.178** (10% Ni, 10% Na$_2$CO$_3$/Al$_2$O$_3$)	Easier CO$_2$ release and higher methanation capacity when Na$_2$CO$_3$ was used as sorbent	[119]
5% K and La	15% Ni/ZrO$_2$	4.7% CO$_2$/He, 250–450 °C, 5 min	Pure H$_2$, 250–450 °C, 5 min	Not reported	K-promotion greatly enhanced CO$_2$ adsorption and promoted methanation at higher temperatures, while La-promotion favoured faster methanation kinetics	[120]
15–30% Mg	17–50% Ni/MgO-Al$_2$O$_3$	15% CO$_2$/N$_2$, 200 and 250 °C, various times	Pure H$_2$, 200 and 250 °C, various times	Not reported	Hydrotalcite-derived layered oxides with high Ni and Mg contents provided a high CH$_4$ yield and favourable methanation kinetics	[121]

3.4. Configuartions Using a Seperate Sorbent and Methanation Catalyst

Apart from the use of a single solid that incorporates both sorption and methanation functions, the process of integrated CO_2 capture and conversion to methane can be realized via the combination of two different solids that perform these functions individually. Veselovskaya et al. published a number of works that incorporated the use of a K_2CO_3/Al_2O_3 sorbent and a Ru/Al_2O_3 methanation catalyst [126–128]. The high CO_2 sorption capabilities of the K_2CO_3-based sorbent enabled it to capture CO_2 directly from ambient air (direct air capture or DAC), where its concentration is as low as 400 ppm. The sorbent could be regenerated at the mild temperature of 200 °C under H_2 flow and CH_4 was produced at a subsequent catalytic reactor that contained the Ru/Al_2O_3 methanation catalyst. The whole operation was coined as direct air capture and methanation (DACM) process [128].

Finally, Miguel et al. [129] also operated the CO_2 capture and conversion to SNG process by using a single reactor that contained alternating layers of the sorbent and catalyst materials. CO_2 sorption was performed by a K-promoted hydrotalcite, whereas a commercial Ni-rich material was used as the methanation catalyst. It was shown that the whole amount of captured CO_2 could be fully hydrogenated into CH_4 and that CH_4 production under cyclic operation was quite high, peaking at 2.36 mol CH_4 per kilogram material and hour of operation.

4. Conclusions

Given the continuous increase of humanity's energy needs and the depletion of our fossil fuel deposits, better management of existing carbon resources via the cyclic conversion between carbon's highest (CO_2) and lowest (CH_4) oxidation state is of particular importance towards the transition to a renewable energy-based economy.

Alkali and alkaline earth metal addition appears to greatly impact the CO_2 methanation activity of supported metal catalysts. Their promoting effect mainly rests on the enhancement of support alkalinity that promotes CO_2 chemisorption, the generation of oxygen vacancies on the surface of metal oxide supports and the improvement of active metal dispersion. Being extremely cheap and earth-abundant, group I and II metals seem to be a viable choice to for use as catalyst promoters towards enhancing the low-temperature activity of Ni-based catalysts, or allowing for a lower noble metal loading (e.g., Ru), without compromising the catalytic activity.

It is, however, evident that, under specific conditions, alkali and sometimes alkaline earth metal addition can suppress methanation activity. This can be achieved by the masking of some active metal sites, for example when impregnating the alkaline modifier after the active metal, or by a detrimental change in the reaction pathway, for example, through a strong interaction with formate intermediates or the increased production of easy-to-desorb CO. More detailed studies on the effect of different alkali and alkaline earth metal promoters on already active methanation catalysts (such as benchmark Ni/CeO_2 and Ni/Al_2O_3) should be undertaken to further clarify their promotion function. In general, it appears that alkaline earths constitute reliable promoters, while the existing literature on promotion with heavier group II metals (Sr and Ba) is comparatively scarce.

The development of new dual-function materials (DFMs) functioning as both catalysts and adsorbents towards the combined CO_2 capture and methanation appears capable of improving the process and as a result, research efforts towards the preparation of such novel materials have boomed during the last 5 years. The main issues that need to be resolved concern the enhancement of the CO_2 sorption capacity and CH_4 production (mostly measured in mmol CH_4/g DFM), as well as the active metal stability under industrial-like flue-gas applications.

However, since the field is quite new and has great potential, many possible research directions do exist. These could include the comparative study of different support materials (e.g., Al_2O_3, SiO_2, ZrO_2, CeO_2 and mesoporous silicas), the employment of additional catalyst synthesis methods (e.g., hydrotalcite-derived catalysts by coprecipitation), the further use of other promoter elements that favour CO_2 adsorption (e.g., La, Sr) and the fabrication of DFMs with stable bimetallic nickel-based catalysts with other transition metals (e.g., NiFe and NiCo alloys).

References

1. Mardani, A.; Streimikiene, D.; Cavallaro, F.; Loganathan, N.; Khoshnoudi, M. Carbon dioxide (CO_2) emissions and economic growth: A systematic review of two decades of research from 1995 to 2017. *Sci. Total Environ.* **2019**, *649*, 31–49. [CrossRef]

2. Szulejko, J.E.; Kumar, P.; Deep, A.; Kim, K.H. Global warming projections to 2100 using simple CO_2 greenhouse gas modeling and comments on CO_2 climate sensitivity factor. *Atmos. Pollut. Res.* **2017**, *8*, 136–140. [CrossRef]

3. Yentekakis, I.V.; Dong, F. Grand challenges for Catalytic Remediation in environmental and energy applications towards a cleaner and sustainable future. *Front. Environ. Chem.* **2020**, *1*, 5. [CrossRef]

4. L'Orange Seigo, S.; Dohle, S.; Siegrist, M. Public perception of carbon capture and storage (CCS): A review. *Renew. Sustain. Energy Rev.* **2014**, *38*, 848–863. [CrossRef]

5. Al-Mamoori, A.; Krishnamurthy, A.; Rownaghi, A.A.; Rezaei, F. Carbon capture and utilization update. *Energy Technol.* **2017**, *5*, 834–849. [CrossRef]

6. Li, W.; Wang, H.; Jiang, X.; Zhu, J.; Liu, Z.; Guo, X.; Song, C. A short review of recent advances in CO_2 hydrogenation to hydrocarbons over heterogeneous catalysts. *RSC Adv.* **2018**, *8*, 7651–7669. [CrossRef]

7. Thema, M.; Bauer, F.; Sterner, M. Power-to-Gas: Electrolysis and methanation status review. *Renew. Sustain. Energy Rev.* **2019**, *112*, 775–787. [CrossRef]

8. Frontera, P.; Macario, A.; Ferraro, M.; Antonucci, P.L. Supported catalysts for CO_2 methanation: A review. *Catalysts* **2017**, *7*, 59. [CrossRef]

9. Vogt, C.; Monai, M.; Kramer, G.J.; Weckhuysen, B.M. The renaissance of the Sabatier reaction and its applications on Earth and in space. *Nat. Catal.* **2019**, *2*, 188–197. [CrossRef]

10. Daza, Y.A.; Kuhn, J.N. CO_2 conversion by reverse water gas shift catalysis: Comparison of catalysts, mechanisms and their consequences for CO_2 conversion to liquid fuels. *RSC Adv.* **2016**, *6*, 49675–49691. [CrossRef]

11. Ye, R.P.; Ding, J.; Gong, W.; Argyle, M.D.; Zhong, Q.; Wang, Y.; Russell, C.K.; Xu, Z.; Russell, A.G.; Li, Q.; et al. CO_2 hydrogenation to high-value products via heterogeneous catalysis. *Nat. Commun.* **2019**, *10*, 1–15. [CrossRef] [PubMed]

12. Vogt, C.; Monai, M.; Sterk, E.B.; Palle, J.; Melcherts, A.E.M.; Zijlstra, B.; Groeneveld, E.; Berben, P.H.; Boereboom, J.M.; Hensen, E.J.M.; et al. Understanding carbon dioxide activation and carbon–carbon coupling over nickel. *Nat. Commun.* **2019**, *10*, 1–10. [CrossRef] [PubMed]

13. Miao, B.; Ma, S.S.K.; Wang, X.; Su, H.; Chan, S.H. Catalysis mechanisms of CO_2 and CO methanation. *Catal. Sci. Technol.* **2016**, *6*, 4048–4058. [CrossRef]

14. Cárdenas-Arenas, A.; Quindimil, A.; Davó-Quiñonero, A.; Bailón-García, E.; Lozano-Castelló, D.; De-La-Torre, U.; Pereda-Ayo, B.; González-Marcos, J.A.; González-Velasco, J.R.; Bueno-López, A. Isotopic and in situ DRIFTS study of the CO_2 methanation mechanism using Ni/CeO_2 and Ni/Al_2O_3 catalysts. *Appl. Catal. B Environ.* **2020**, *265*, 118538. [CrossRef]

15. Tada, S.; Shimizu, T.; Kameyama, H.; Haneda, T.; Kikuchi, R. Ni/CeO_2 catalysts with high CO_2 methanation activity and high CH_4 selectivity at low temperatures. *Int. J. Hydrog. Energy* **2012**, *37*, 5527–5531. [CrossRef]

16. Boaro, M.; Colussi, S.; Trovarelli, A. Ceria-based materials in hydrogenation and reforming reactions for CO_2 valorization. *Front. Chem.* **2019**, *7*, 28. [CrossRef]

17. Choi, S.; Drese, J.H.; Jones, C.W. Adsorbent materials for carbon dioxide capture from large anthropogenic point sources. *ChemSusChem* **2009**, *2*, 796–854. [CrossRef]

18. Kierzkowska, A.M.; Pacciani, R.; Müller, C.R. CaO-based CO_2 sorbents: From fundamentals to the development of new, highly effective materials. *ChemSusChem* **2013**, *6*, 1130–1148. [CrossRef]

19. Duyar, M.S.; Arellano-Treviño, M.A.; Farrauto, R.J. Dual function materials for CO_2 capture and conversion using renewable H_2. *Appl. Catal. B Environ.* **2015**, *168–169*, 370–376. [CrossRef]

20. Melo Bravo, P.; Debecker, D.P. Combining CO_2 capture and catalytic conversion to methane. *Waste Dispos. Sustain. Energy* **2019**, *1*, 53–65. [CrossRef]

21. Arellano-Treviño, M.A.; He, Z.; Libby, M.C.; Farrauto, R.J. Catalysts and adsorbents for CO_2 capture and conversion with dual function materials: Limitations of Ni-containing DFMs for flue gas applications. *J. CO_2 Util.* **2019**, *31*, 143–151. [CrossRef]

22. Wang, S.; Schrunk, E.T.; Mahajan, H.; Farrauto, R.J. The role of ruthenium in CO_2 capture and catalytic conversion to fuel by dual function materials (DFM). *Catalysts* **2017**, *7*, 88. [CrossRef]

23. Arellano-Treviño, M.A.; Kanani, N.; Jeong-Potter, C.W.; Farrauto, R.J. Bimetallic catalysts for CO_2 capture and hydrogenation at simulated flue gas conditions. *Chem. Eng. J.* **2019**, *375*, 121953. [CrossRef]

24. Bermejo-López, A.; Pereda-Ayo, B.; González-Marcos, J.A.; González-Velasco, J.R. Mechanism of the CO_2 storage and in situ hydrogenation to CH_4. Temperature and adsorbent loading effects over $Ru-CaO/Al_2O_3$ and $Ru-Na_2CO_3/Al_2O_3$ catalysts. *Appl. Catal. B Environ.* **2019**, *256*, 117845. [CrossRef]

25. Sun, H.; Zhang, Y.; Guan, S.; Huang, J.; Wu, C. Direct and highly selective conversion of captured CO_2 into methane through integrated carbon capture and utilization over dual functional materials. *J. CO_2 Util.* **2020**, *38*, 262–272. [CrossRef]

26. Aziz, M.A.A.; Jalil, A.A.; Triwahyono, S.; Ahmad, A. CO_2 methanation over heterogeneous catalysts: Recent progress and future prospects. *Green Chem.* **2015**, *17*, 2647–2663. [CrossRef]

27. Lee, W.J.; Li, C.; Prajitno, H.; Yoo, J.; Patel, J.; Yang, Y.; Lim, S. Recent trend in thermal catalytic low temperature CO_2 methanation: A critical review. *Catal. Today* **2020**, in press. [CrossRef]

28. Lv, C.; Xu, L.; Chen, M.; Cui, Y.; Wen, X.; Li, Y.; Wu, C.E.; Yang, B.; Miao, Z.; Hu, X.; et al. Recent Progresses in Constructing the Highly Efficient Ni Based Catalysts With Advanced Low-Temperature Activity Toward CO_2 Methanation. *Front. Chem.* **2020**, *8*, 1–32. [CrossRef]

29. Charisiou, N.D.; Siakavelas, G.; Tzounis, L.; Sebastian, V.; Monzon, A.; Baker, M.A.; Hinder, S.J.; Polychronopoulou, K.; Yentekakis, I.V.; Goula, M.A. An in depth investigation of deactivation through carbon formation during the biogas dry reforming reaction for Ni supported on modified with CeO_2 and La_2O_3 zirconia catalysts. *Int. J. Hydrog. Energy* **2018**, *43*, 18955–18976. [CrossRef]

30. Liu, K.; Xu, X.; Xu, J.; Fang, X.; Liu, L.; Wang, X. The distributions of alkaline earth metal oxides and their promotional effects on Ni/CeO_2 for CO_2 methanation. *J. CO_2 Util.* **2020**, *38*, 113–124. [CrossRef]

31. Charisiou, N.D.; Baklavaridis, A.; Papadakis, V.G.; Goula, M.A. Synthesis Gas Production via the Biogas Reforming Reaction Over $Ni/MgO–Al_2O_3$ and $Ni/CaO–Al_2O_3$ Catalysts. *Waste Biomass Valorization* **2016**, *7*, 725–736. [CrossRef]

32. Yentekakis, I.V.; Vernoux, P.; Goula, G.; Caravaca, A. Electropositive promotion by alkalis or alkaline earths of Pt-group metals in emissions control catalysis: A status report. *Catalysts* **2019**, *9*, 157. [CrossRef]

33. Petala, A.; Panagiotopoulou, P. Methanation of CO_2 over alkali-promoted Ru/TiO_2 catalysts: I. Effect of alkali additives on catalytic activity and selectivity. *Appl. Catal. B Environ.* **2018**, *224*, 919–927. [CrossRef]

34. Panagiotopoulou, P. Methanation of CO_2 over alkali-promoted Ru/TiO_2 catalysts: II. Effect of alkali additives on the reaction pathway. *Appl. Catal. B Environ.* **2018**, *236*, 162–170. [CrossRef]

35. Cimino, S.; Boccia, F.; Lisi, L. Effect of alkali promoters (Li, Na, K) on the performance of Ru/Al_2O_3 catalysts for CO_2 capture and hydrogenation to methane. *J. CO_2 Util.* **2020**, *37*, 195–203. [CrossRef]

36. Liang, C.; Ye, Z.; Dong, D.; Zhang, S.; Liu, Q.; Chen, G.; Li, C.; Wang, Y.; Hu, X. Methanation of CO_2: Impacts of modifying nickel catalysts with variable-valence additives on reaction mechanism. *Fuel* **2019**, *254*, 115654. [CrossRef]

37. Zhang, Z.; Zhang, X.; Zhang, L.; Gao, J.; Shao, Y.; Dong, D.; Zhang, S.; Liu, Q.; Xu, L.; Hu, X. Impacts of alkali or alkaline earth metals addition on reaction intermediates formed in methanation of CO_2 over cobalt catalysts. *J. Energy Inst.* **2020**, *93*, 1581–1596. [CrossRef]

38. Vayenas, C.G.; Bebelis, S.; Yentekakis, I.V.; Lintz, H.G. Non-faradaic electrochemical modification of catalytic activity: A status report. *Catal. Today* **1992**, *11*, 303–438. [CrossRef]

39. Klaitzidou, I.; Makri, M.; Theleritis, D.; Katsaounis, A.; Vayenas, C.G. Comparative study of the electrochemical promotion of CO_2 hydrogenation on Ru using Na^+, K^+, H^+ and O^{2-} conducting solid electrolytes. *Surf. Sci.* **2016**, *646*, 194–203. [CrossRef]

40. Theleritis, D.; Makri, M.; Souentie, S.; Caravaca, A.; Katsaounis, A.; Vayenas, C.G. Comparative study of the electrochemical promotion of CO_2 hydrogenation over Ru-supported catalysts using electronegative and electropositive promoters. *ChemElectroChem* **2014**, *1*, 254–262. [CrossRef]

41. Le, T.A.; Kim, T.W.; Lee, S.H.; Park, E.D. Effects of Na content in $Na/Ni/SiO_2$ and $Na/Ni/CeO_2$ catalysts for CO and CO_2 methanation. *Catal. Today* **2018**, *303*, 159–167. [CrossRef]

42. Beierlein, D.; Häussermann, D.; Pfeifer, M.; Schwarz, T.; Stöwe, K.; Traa, Y.; Klemm, E. Is the CO_2 methanation on highly loaded $Ni-Al_2O_3$ catalysts really structure-sensitive? *Appl. Catal. B Environ.* **2019**, *247*, 200–219. [CrossRef]

43. Büchel, R.; Baiker, A.; Pratsinis, S.E. Effect of Ba and K addition and controlled spatial deposition of Rh in Rh/Al_2O_3 catalysts for CO_2 hydrogenation. *Appl. Catal. A Gen.* **2014**, *477*, 93–101. [CrossRef]

44. Iloy, R.A.; Jalama, K. Effect of Operating Temperature, Pressure and Pottasium Loading on the Performance of Silica-Supported Cobalt Catalyst in CO_2 Hydrogenation to Hydrocarbon Fuel. *Catalysts* **2019**, *9*, 807. [CrossRef]

45. Zhang, Z.; Hu, X.; Wang, Y.; Hu, S.; Xiang, J.; Li, C.; Chen, G.; Liu, Q.; Wei, T.; Dong, D. Regulation the reaction intermediates in methanation reactions via modification of nickel catalysts with strong base. *Fuel* **2019**, *237*, 566–579. [CrossRef]

46. He, L.; Lin, Q.; Liu, Y.; Huang, Y. Unique catalysis of Ni-Al hydrotalcite derived catalyst in CO_2 methanation: Cooperative effect between Ni nanoparticles and a basic support. *J. Energy Chem.* **2014**, *23*, 587–592. [CrossRef]

47. Konsolakis, M.; Yentekakis, I.V. Strong promotional effects of Li, K, Rb and Cs on the Pt-catalysed reduction of NO by propene. *Appl. Catal. B* **2001**, *29*, 103–113. [CrossRef]

48. Yentekakis, I.V.; Konsolakis, M.; Lambert, R.M.; Palermo, A.; Tikhov, M. Successful application of the electrochemical promotion to the design of effective conventional catalyst formulations. *Solid State Ion.* **2000**, *136*, 783–790. [CrossRef]

49. Vogt, C.; Wijten, J.; Madeira, C.L.; Kerkenaar, O.; Xu, K.; Holzinger, R.; Monai, M.; Weckhuysen, B.M. Alkali Promotion in the Formation of CH_4 from CO_2 and Renewably Produced H_2 over Supported Ni Catalysts. *ChemCatChem* **2020**, *12*, 2792–2800. [CrossRef]

50. Yang, Q.; Liu, G.; Liu, Y. Perovskite-Type Oxides as the Catalyst Precursors for Preparing Supported Metallic Nanocatalysts: A Review. *Ind. Eng. Chem. Res.* **2018**, *57*, 1–17. [CrossRef]

51. Tsounis, C.; Wang, Y.; Arandiyan, H.; Wong, R.J.; Toe, C.Y.; Amal, R.; Scott, J. Tuning the Selectivity of $LaNiO_3$ Perovskites for CO_2 hydrogenation through potassium substitution. *Catalysts* **2020**, *10*, 409. [CrossRef]

52. Guo, M.; Lu, G. The difference of roles of alkaline-earth metal oxides on silica-supported nickel catalysts for CO_2 methanation. *RSC Adv.* **2014**, *4*, 58171–58177. [CrossRef]

53. Liang, C.; Hu, X.; Wei, T.; Jia, P.; Zhang, Z.; Dong, D.; Zhang, S.; Liu, Q.; Hu, G. Methanation of CO_2 over Ni/Al_2O_3 modified with alkaline earth metals: Impacts of oxygen vacancies on catalytic activity. *Int. J. Hydrog. Energy* **2019**, *44*, 8197–8213. [CrossRef]

54. Yentekakis, I.V.; Goula, G.; Hatzisymeon, M.; Betsi-Argyropoulou, I.; Botzolaki, G.; Kousi, K.; Kondarides, D.I.; Taylor, M.J.; Parlett, C.M.A.; Osatiashtiani, A.; et al. Effect of support oxygen storage capacity on the catalytic performance of Rh nanoparticles for CO_2 reforming of methane. *Appl. Catal. B Environ.* **2019**, *243*, 490–501. [CrossRef]

55. Goula, M.A.; Charisiou, N.D.; Siakavelas, G.; Tzounis, L.; Tsiaoussis, I.; Panagiotopoulou, P.; Goula, G.; Yentekakis, I.V. Syngas production via the biogas dry reforming reaction over Ni supported on zirconia modified with CeO_2 or La_2O_3 catalysts. *Int. J. Hydrog. Energy* **2017**, *42*, 13724–13740. [CrossRef]

56. Huang, J.; Li, X.; Wang, X.; Fang, X.; Wang, H.; Xu, X. New insights into CO_2 methanation mechanisms on Ni/MgO catalysts by DFT calculations: Elucidating Ni and MgO roles and support effects. *J. CO_2 Util.* **2019**, *33*, 55–63. [CrossRef]

57. Li, Y.; Lu, G.; Ma, J. Highly active and stable nano NiO-MgO catalyst encapsulated by silica with a core-shell structure for CO_2 methanation. *RSC Adv.* **2014**, *4*, 17420–17428. [CrossRef]

58. Park, J.N.; McFarland, E.W. A highly dispersed $Pd-Mg/SiO_2$ catalyst active for methanation of CO_2. *J. Catal.* **2009**, *266*, 92–97. [CrossRef]

59. Kim, H.Y.; Lee, H.M.; Park, J.N. Bifunctional mechanism of CO_2 methanation on Pd-MgO/SiO_2 catalyst: Independent roles of MgO and Pd on CO_2 methanation. *J. Phys. Chem. C* **2010**, *114*, 7128–7131. [CrossRef]

60. Kwak, J.H.; Kovarik, L.; Szanyi, J. Heterogeneous catalysis on atomically dispersed supported metals: CO_2 reduction on multifunctional Pd catalysts. *ACS Catal.* **2013**, *3*, 2094–2100. [CrossRef]

61. Alcalde-Santiago, V.; Davó-Quiñonero, A.; Lozano-Castelló, D.; Quindimil, A.; De-La-Torre, U.; Pereda-Ayo, B.; González-Marcos, J.A.; González-Velasco, J.R.; Bueno-López, A. Ni/LnO_x catalysts (Ln = La, Ce or Pr) for CO_2 methanation. *ChemCatChem* **2019**, *11*, 810–819.

62. Cárdenas-Arenas, A.; Quindimil, A.; Davó-Quinonero, A.; Bailón-García, E.; Lozano-Castelló, D.; De-La-Torre, U.; Pereda-Ayo, B.; González-Marcos, J.A.; González-Velasco, J.R.; Bueno-López, A. Design of active sites in Ni/CeO_2 catalysts for the methanation of CO_2: Tailoring the Ni-CeO_2 contact. *Appl. Mater. Today* **2020**, *19*, 100591. [CrossRef]

63. Guo, M.; Lu, G. The effect of impregnation strategy on structural characters and CO_2 methanation properties over MgO modified Ni/SiO_2 catalysts. *Catal. Commun.* **2014**, *54*, 55–60. [CrossRef]

64. Tan, J.; Wang, J.; Zhang, Z.; Ma, Z.; Wang, L.; Liu, Y. Highly dispersed and stable Ni nanoparticles confined by MgO on ZrO_2 for CO_2 methanation. *Appl. Surf. Sci.* **2019**, *481*, 1538–1548. [CrossRef]

65. Xu, L.; Wang, F.; Chen, M.; Yang, H.; Nie, D.; Qi, L.; Lian, X. Alkaline-promoted Ni based ordered mesoporous catalysts with enhanced low-temperature catalytic activity toward CO_2 methanation. *RSC Adv.* **2017**, *7*, 18199–18210. [CrossRef]

66. Li, X.; Wang, Y.; Zhang, G.; Sun, W.; Bai, Y.; Zheng, L.; Han, X.; Wu, L. Influence of Mg-promoted Ni-based Catalyst Supported on Coconut Shell Carbon for CO_2 Methanation. *ChemistrySelect* **2019**, *4*, 838–845. [CrossRef]

67. Xiao-liu, W.; Meng, Y.; Ling-jun, Z.; Xiao-nan, Z.; Shu-rong, W. CO_2 methanation over Ni /Mg@MCM-41 prepared by in-situ synthesis method. *J. Fuel Chem. Technol.* **2020**, *48*, 456–465.

68. Bacariza, M.C.; Graça, I.; Bebiano, S.S.; Lopes, J.M.; Henriques, C. Magnesium as Promoter of CO_2 Methanation on Ni-Based USY Zeolites. *Energy Fuels* **2017**, *31*, 9776–9789. [CrossRef]

69. Yang, H.; Xu, L.; Chen, M.; Lv, C.; Cui, Y.; Wen, X.; Wu, C.E.; Yang, B.; Miao, Z.; Hu, X.; et al. Facilely fabricating highly dispersed Ni-based catalysts supported on mesoporous MFI nanosponge for CO_2 methanation. *Microporous Mesoporous Mater.* **2020**, *302*, 110250. [CrossRef]

70. Zhang, L.; Bian, L.; Zhu, Z.; Li, Z. La-promoted Ni/Mg-Al catalysts with highly enhanced low-temperature CO_2 methanation performance. *Int. J. Hydrog. Energy* **2018**, *43*, 2197–2206. [CrossRef]

71. Jingyu, Z.; Hongfang, M.; Fangyu, J.; Haitao, Z.; Weiyong, Y. Mn and Mg dual promoters modified Ni/α-Al_2O_3 catalysts for high temperature syngas methanation. *Fuel Process. Technol.* **2018**, *172*, 225–232.

72. Baysal, Z.; Kureti, S. CO_2 methanation on Mg-promoted Fe catalysts. *Appl. Catal. B Environ.* **2020**, *262*, 118300. [CrossRef]

73. Kirchner, J.; Baysal, Z.; Kureti, S. Activity and Structural Changes of Fe-based Catalysts during CO_2 Hydrogenation towards CH_4—A Mini Review. *ChemCatChem* **2020**, *12*, 981–988. [CrossRef]

74. Xu, L.; Yang, H.; Chen, M.; Wang, F.; Nie, D.; Qi, L.; Lian, X.; Chen, H.; Wu, M. CO_2 methanation over Ca doped ordered mesoporous Ni-Al composite oxide catalysts: The promoting effect of basic modifier. *J. CO_2 Util.* **2017**, *21*, 200–210. [CrossRef]

75. Liu, Q.; Wang, S.; Zhao, G.; Yang, H.; Yuan, M.; An, X.; Zhou, H.; Qiao, Y.; Tian, Y. CO_2 methanation over ordered mesoporous NiRu-doped CaO-Al_2O_3 nanocomposites with enhanced catalytic performance. *Int. J. Hydrog. Energy* **2018**, *43*, 239–250. [CrossRef]

76. Do, P.N.U.; Luu, C.L.; Nguyen, P.A.; Van Nguyen, T.T.; Hoang, T.C.; Nguyen, T. Promotion effect of CO on methanation of CO_2-rich gas over nanostructured modified NiO/γ-Al_2O_3 catalysts. *Adv. Nat. Sci. Nanosci. Nanotechnol.* **2019**, *10*, 035004. [CrossRef]

77. Yang, W.; Feng, Y.; Chu, W. Promotion effect of CaO modification on mesoporous Al_2O_3-supported Ni catalysts for CO_2 methanation. *Int. J. Chem. Eng.* **2016**, *2016*, 2041821. [CrossRef]

78. Hu, X.F.; Yang, W.; Wang, N.; Luo, S.Z.; Chu, W. Catalytic properties of Ni/CNTs and Ca-Promoted Ni/CNTs for methanation reaction of carbon dioxide. *Adv. Mater. Res.* **2014**, *924*, 217–226. [CrossRef]

79. Feng, Y.; Yang, W.; Chu, W. Effect of Ca modification on the catalytic performance of Ni/AC for CO_2 methanation. *Integr. Ferroelectr.* **2016**, *172*, 40–48. [CrossRef]

80. Zhou, M.; Ahmad, A. Synthesis, processing and characterization of calcia-stabilized zirconia solid electrolytes for oxygen sensing applications. *Mater. Res. Bull.* **2006**, *41*, 690–696. [CrossRef]

81. Takano, H.; Shinomiya, H.; Izumiya, K.; Kumagai, N.; Habazaki, H.; Hashimoto, K. CO_2 methanation of Ni catalysts supported on tetragonal ZrO_2 doped with Ca^{2+} and Ni^{2+} ions. *Int. J. Hydrog. Energy* **2015**, *40*, 8347–8355. [CrossRef]

82. Everett, O.E.; Zonetti, P.C.; Alves, O.C.; de Avillez, R.R.; Appel, L.G. The role of oxygen vacancies in the CO_2 methanation employing Ni/ZrO_2 doped with Ca. *Int. J. Hydrog. Energy* **2020**, *45*, 6352–6359. [CrossRef]

83. Jia, C.; Gao, J.; Li, J.; Gu, F.; Xu, G.; Zhong, Z.; Su, F. Nickel catalysts supported on calcium titanate for enhanced CO methanation. *Catal. Sci. Technol.* **2013**, *3*, 490–499. [CrossRef]

84. Do, J.Y.; Park, N.K.; Seo, M.W.; Lee, D.; Ryu, H.J.; Kang, M. Effective thermocatalytic carbon dioxide methanation on Ca-inserted $NiTiO_3$ perovskite. *Fuel* **2020**, *271*, 117624. [CrossRef]

85. Toemen, S.; Abu Bakar, W.A.W.; Ali, R. Effect of ceria and strontia over $Ru/Mn/Al_2O_3$ catalyst: Catalytic methanation, physicochemical and mechanistic studies. *J. CO_2 Util.* **2016**, *13*, 38–49. [CrossRef]

86. Steiger, P.; Kröcher, O.; Ferri, D. Increased nickel exsolution from $LaFe_{0.8}Ni_{0.2}O_3$ perovskite-derived CO_2 methanation catalysts through strontium doping. *Appl. Catal. A Gen.* **2020**, *590*, 117328. [CrossRef]

87. Huynh, H.L.; Yu, Z. CO_2 Methanation on Hydrotalcite-Derived Catalysts and Structured Reactors: A Review. *Energy Technol.* **2020**, *8*, 1901475. [CrossRef]

88. Bacariza, M.C.; Graça, I.; Lopes, J.M.; Henriques, C. Tuning Zeolite Properties towards CO_2 Methanation: An Overview. *ChemCatChem* **2019**, *11*, 2388–2400. [CrossRef]

89. Bette, N.; Thielemann, J.; Schreiner, M.; Mertens, F. Methanation of CO_2 over a $(Mg,Al)O_x$ Supported Nickel Catalyst Derived from a (Ni,Mg,Al)-Hydrotalcite-like Precursor. *ChemCatChem* **2016**, *8*, 2903–2906. [CrossRef]

90. Liu, J.; Bing, W.; Xue, X.; Wang, F.; Wang, B.; He, S.; Zhang, Y.; Wei, M. Alkaline-assisted Ni nanocatalysts with largely enhanced low-temperature activity toward CO_2 methanation. *Catal. Sci. Technol.* **2016**, *6*, 3976–3983. [CrossRef]

91. Ren, J.; Mebrahtu, C.; Palkovits, R. Ni-based catalysts supported on Mg-Al hydrotalcites with different morphologies for CO_2 methanation: Exploring the effect of metal-support interaction. *Catal. Sci. Technol.* **2020**, *10*, 1902–1913. [CrossRef]

92. Wierzbicki, D.; Debek, R.; Motak, M.; Grzybek, T.; Gálvez, M.E.; Da Costa, P. Novel Ni-La-hydrotalcite derived catalysts for CO_2 methanation. *Catal. Commun.* **2016**, *83*, 5–8. [CrossRef]

93. Wierzbicki, D.; Motak, M.; Grzybek, T.; Gálvez, M.E.; Da Costa, P. The influence of lanthanum incorporation method on the performance of nickel-containing hydrotalcite-derived catalysts in CO_2 methanation reaction. *Catal. Today* **2018**, *307*, 205–211. [CrossRef]

94. Martins, J.A.; Faria, A.C.; Soria, M.A.; Miguel, C.V.; Rodrigues, A.E.; Madeira, L.M. CO_2 methanation over hydrotalcite-derived nickel/ruthenium and supported ruthenium catalysts. *Catalysts* **2019**, *9*, 1008. [CrossRef]

95. Mebrahtu, C.; Krebs, F.; Perathoner, S.; Abate, S.; Centi, G.; Palkovits, R. Hydrotalcite based Ni-Fe/$(Mg, Al)O_x$ catalysts for CO_2 methanation-tailoring Fe content for improved CO dissociation, basicity, and particle size. *Catal. Sci. Technol.* **2018**, *8*, 1016–1027. [CrossRef]

96. Graça, I.; González, L.V.; Bacariza, M.C.; Fernandes, A.; Henriques, C.; Lopes, J.M.; Ribeiro, M.F. CO_2 hydrogenation into CH_4 on NiHNaUSY zeolites. *Appl. Catal. B Environ.* **2014**, *147*, 101–110. [CrossRef]

97. Westermann, A.; Azambre, B.; Bacariza, M.C.; Graça, I.; Ribeiro, M.F.; Lopes, J.M.; Henriques, C. Insight into CO_2 methanation mechanism over NiUSY zeolites: An operando IR study. *Appl. Catal. B Environ.* **2015**, *174*, 120–125. [CrossRef]

98. Bacariza, M.C.; Bértolo, R.; Graça, I.; Lopes, J.M.; Henriques, C. The effect of the compensating cation on the catalytic performances of Ni/USY zeolites towards CO_2 methanation. *J. CO_2 Util.* **2017**, *21*, 280–291. [CrossRef]

99. Bacariza, M.C.; Graça, I.; Lopes, J.M.; Henriques, C. Enhanced activity of CO_2 hydrogenation to CH_4 over Ni based zeolites through the optimization of the Si/Al ratio. *Microporous Mesoporous Mater.* **2018**, *267*, 9–19. [CrossRef]

100. Quindimil, A.; De-La-Torre, U.; Pereda-Ayo, B.; González-Marcos, J.A.; González-Velasco, J.R. Ni catalysts with La as promoter supported over Y- and BETA- zeolites for CO_2 methanation. *Appl. Catal. B Environ.* **2018**, *238*, 393–403. [CrossRef]

101. Bacariza, M.C.; Graça, I.; Lopes, J.M.; Henriques, C. Ni-Ce/Zeolites for CO_2 Hydrogenation to CH_4: Effect of the Metal Incorporation Order. *ChemCatChem* **2018**, *10*, 2773–2781. [CrossRef]

102. Zhang, F.; Lu, B.; Sun, P. Highly stable Ni-based catalysts derived from LDHs supported on zeolite for CO_2 methanation. *Int. J. Hydrog. Energy* **2020**, *45*, 16183–16192. [CrossRef]

103. Xu, L.; Wang, F.; Chen, M.; Nie, D.; Lian, X.; Lu, Z.; Chen, H.; Zhang, K.; Ge, P. CO_2 methanation over rare earth doped Ni based mesoporous catalysts with intensified low-temperature activity. *Int. J. Hydrog. Energy* **2017**, *42*, 15523–15539. [CrossRef]

104. Zhao, K.; Li, Z.; Bian, L. CO_2 methanation and co-methanation of CO and CO_2 over Mn-promoted Ni/Al_2O_3 catalysts. *Front. Chem. Sci. Eng.* **2016**, *10*, 273–280. [CrossRef]

105. Liu, Q.; Bian, B.; Fan, J.; Yang, J. Cobalt doped Ni based ordered mesoporous catalysts for CO_2 methanation with enhanced catalytic performance. *Int. J. Hydrog. Energy* **2018**, *43*, 4893–4901. [CrossRef]

106. Mihet, M.; Lazar, M.D. Methanation of CO_2 on Ni/γ-Al_2O_3: Influence of Pt, Pd or Rh promotion. *Catal. Today* **2018**, *306*, 294–299. [CrossRef]

107. Guilera, J.; Del Valle, J.; Alarcón, A.; Díaz, J.A.; Andreu, T. Metal-oxide promoted Ni/Al_2O_3 as CO_2 methanation micro-size catalysts. *J. CO_2 Util.* **2019**, *30*, 11–17. [CrossRef]

108. Garbarino, G.; Wang, C.; Cavattoni, T.; Finocchio, E.; Riani, P.; Flytzani-Stephanopoulos, M.; Busca, G. A study of Ni/La-Al_2O_3 catalysts: A competitive system for CO_2 methanation. *Appl. Catal. B Environ.* **2019**, *248*, 286–297. [CrossRef]

109. Liang, C.; Wei, T.; Wang, H.; Yu, Z.; Dong, D.; Zhang, S.; Liu, Q.; Hu, G.; Hu, X. Impacts of La addition on formation of the reaction intermediates over alumina and silica supported nickel catalysts in methanation of CO_2. *J. Energy Inst.* **2020**, *93*, 723–738. [CrossRef]

110. Wang, X.; Zhu, L.; Zhuo, Y.; Zhu, Y.; Wang, S. Enhancement of CO_2 Methanation over La-Modified Ni/SBA-15 Catalysts Prepared by Different Doping Methods. *ACS Sustain. Chem. Eng.* **2019**, *7*, 14647–14660. [CrossRef]

111. Zhang, T.; Liu, Q. Perovskite $LaNiO_3$ Nanocrystals inside Mesostructured Cellular Foam Silica: High Catalytic Activity and Stability for CO_2 Methanation. *Energy Technol.* **2020**, *8*, 1–12. [CrossRef]

112. Bermejo-López, A.; Pereda-Ayo, B.; González-Marcos, J.A.; González-Velasco, J.R. Ni loading effects on dual function materials for capture and in-situ conversion of CO_2 to CH_4 using CaO or Na_2CO_3. *J. CO_2 Util.* **2019**, *34*, 576–587. [CrossRef]

113. Duyar, M.S.; Wang, S.; Arellano-Treviño, M.A.; Farrauto, R.J. CO_2 utilization with a novel dual function material (DFM) for capture and catalytic conversion to synthetic natural gas: An update. *J. CO_2 Util.* **2016**, *15*, 65–71. [CrossRef]

114. Zheng, Q.; Farrauto, R.; Chau Nguyen, A. Adsorption and Methanation of Flue Gas CO_2 with Dual Functional Catalytic Materials: A Parametric Study. *Ind. Eng. Chem. Res.* **2016**, *55*, 6768–6776. [CrossRef]

115. Wang, S.; Farrauto, R.J.; Karp, S.; Jeon, J.H.; Schrunk, E.T. Parametric, cyclic aging and characterization studies for CO_2 capture from flue gas and catalytic conversion to synthetic natural gas using a dual functional material (DFM). *J. CO_2 Util.* **2018**, *27*, 390–397. [CrossRef]

116. Proaño, L.; Tello, E.; Arellano-Trevino, M.A.; Wang, S.; Farrauto, R.J.; Cobo, M. In-situ DRIFTS study of two-step CO_2 capture and catalytic methanation over Ru,"Na_2O"/Al_2O_3 Dual Functional Material. *Appl. Surf. Sci.* **2019**, *479*, 25–30. [CrossRef]

117. Wang, F.; He, S.; Chen, H.; Wang, B.; Zheng, L.; Wei, M.; Evans, D.G.; Duan, X. Active Site Dependent Reaction Mechanism over Ru/CeO_2 Catalyst toward CO_2 Methanation. *J. Am. Chem. Soc.* **2016**, *138*, 6298–6305. [CrossRef]

118. Zhen, W.; Li, B.; Lu, G.; Ma, J. Enhancing catalytic activity and stability for CO_2 methanation on Ni–Ru/γ-Al_2O_3 via modulating impregnation sequence and controlling surface active species. *RSC Adv.* **2014**, *4*, 16472–16479. [CrossRef]

119. Chai, K.H.; Leong, L.K.; Wong, D.S.H.; Tsai, D.H.; Sethupathi, S. Effect of CO_2 adsorbents on the Ni-based dual-function materials for CO_2 capturing and in situ methanation. *J. Chin. Chem. Soc.* **2020**, *67*, 1–11. [CrossRef]

120. Hu, L.; Urakawa, A. Continuous CO_2 capture and reduction in one process: CO_2 methanation over unpromoted and promoted Ni/ZrO_2. *J. CO_2 Util.* **2018**, *25*, 323–329. [CrossRef]

121. Zhou, Z.; Sun, N.; Wang, B.; Han, Z.; Cao, S.; Hu, D.; Zhu, T.; Shen, Q.; Wei, W. 2D-Layered Ni–MgO–Al_2O_3 Nanosheets for Integrated Capture and Methanation of CO_2. *ChemSusChem* **2020**, *13*, 360–368. [CrossRef]

122. Bobadilla, L.F.; Riesco-García, J.M.; Penelás-Pérez, G.; Urakawa, A. Enabling continuous capture and catalytic conversion of flue gas CO_2 to syngas in one process. *J. CO_2 Util.* **2016**, *14*, 106–111. [CrossRef]

123. Hyakutake, T.; Van Beek, W.; Urakawa, A. Unravelling the nature, evolution and spatial gradients of active species and active sites in the catalyst bed of unpromoted and K/Ba-promoted Cu/Al_2O_3 during CO_2 capture-reduction. *J. Mater. Chem. A* **2016**, *4*, 6878–6885. [CrossRef]

124. Al-Mamoori, A.; Rownaghi, A.A.; Rezaei, F. Combined Capture and Utilization of CO_2 for Syngas Production over Dual-Function Materials. *ACS Sustain. Chem. Eng.* **2018**, *6*, 13551–13561. [CrossRef]

125. Sun, H.; Wang, J.; Zhao, J.; Shen, B.; Shi, J.; Huang, J.; Wu, C. Dual functional catalytic materials of Ni over Ce-modified CaO sorbents for integrated CO_2 capture and conversion. *Appl. Catal. B Environ.* **2019**, *244*, 63–75. [CrossRef]

126. Veselovskaya, J.V.; Parunin, P.D.; Netskina, O.V.; Kibis, L.S.; Lysikov, A.I.; Okunev, A.G. Catalytic methanation of carbon dioxide captured from ambient air. *Energy* **2018**, *159*, 766–773. [CrossRef]

127. Veselovskaya, J.V.; Parunin, P.D.; Netskina, O.V.; Okunev, A.G. A Novel Process for Renewable Methane Production: Combining Direct Air Capture by K_2CO_3/Alumina Sorbent with CO_2 Methanation over Ru/Alumina Catalyst. *Top. Catal.* **2018**, *61*, 1528–1536. [CrossRef]

128. Veselovskaya, J.V.; Lysikov, A.I.; Netskina, O.V.; Kuleshov, D.V.; Okunev, A.G. K_2CO_3-Containing Composite Sorbents Based on Thermally Modified Alumina: Synthesis, Properties, and Potential Application in a Direct Air Capture/Methanation Process. *Ind. Eng. Chem. Res.* **2020**, *59*, 7130–7139. [CrossRef]

129. Miguel, C.V.; Soria, M.A.; Mendes, A.; Madeira, L.M. A sorptive reactor for CO_2 capture and conversion to renewable methane. *Chem. Eng. J.* **2017**, *322*, 590–602. [CrossRef]